Reconstructing past variations in environmental conditions and paleoproductivity over the last ~8000 years off Central Chile (30° S)

Práxedes Muñoz[1,2], Lorena Rebolledo[3,4], Laurent Dezileau[5], Antonio Maldonado[2], Christoph Mayr[6,7], Paola Cárdenas[4,8], Carina B. Lange[4,9,10], Katherine Lalangui[9], Gloria Sanchez[11], Marco Salamanca[9], Karen Araya[1,5], Ignacio Jara[2], Gabriel Vargas[12], Marcel Ramos[1,2].

[1]Departamento de Biología Marina, Universidad Católica del Norte, Larrondo 1281, Coquimbo, Chile.
[2]Centro de Estudios Avanzados en Zonas Áridas (CEAZA), Coquimbo-La Serena, Chile.
[3]Departamento Científico, Instituto Antártico Chileno, Punta Arenas, Chile.
[4]Centro FONDAP de Investigación Dinámica de Ecosistemas Marinos de Altas Latitudes (IDEAL), Universidad Austral de Chile, Campus Isla Teja, Valdivia, Chile.
[5]Laboratoire Géosciences Montpellier (GM), Université de Montpellier, 34095 Montpellier Cedex 05, France.
[6]Institut für Geographie, FAU Erlangen-Nürnberg, 91058 Erlangen, Germany.
[7]Department of Earth and Environmental Sciences & GeoBio-Center, LMU Munich, 80333 Munich.
[8]Programa Magister en Oceanografía, Universidad de Concepción, casilla 160C, Concepción, Chile.
[9]Departamento de Oceanografía, Facultad de Ciencias Naturales y Oceanográficas, Universidad de Concepción, Casilla 160C, Concepción, Chile.
[10]Centro de Investigación Oceanográfica COPAS Sur-Austral, Universidad de Concepción, Casilla 160C, Concepción, Chile.
[11]Universidad de Magallanes, Punta Arenas, Chile.
[12]Departamento de Geología, Universidad de Chile, Santiago, Chile.

Correspondence: Práxedes Muñoz (praxedes@ucn.cl)

Abstract

The Coquimbo (30°S) region, in the North-central Chilean Coast, is characterized by relative dry summers and a short rainfall period during winter months. The wet-winter climate results from the interactions between the Southern Westerly Winds and the South Pacific Anticyclone (SPA). Interdecadal climate trends are mostly associated with El Niño-Southern Oscillation (ENSO), which produces high variability in precipitation. With the aim of establishing past variations of the main oceanographic and climatic features in the Central Chilean coast, we analyze recent sedimentary records of a transitional semi-arid ecosystem susceptible to environmental forcing conditions. Sediment cores were retrieved in two bays, Guanaqueros and Tongoy (29−30°S), for geochemical analyses including: sensitive redox trace elements, biogenic opal, total organic carbon (TOC), diatoms, stable isotopes of organic carbon and nitrogen. Three main periods of increased productivity were established: (1) > cal BP 6500, (2) cal BP 2000 – cal BP 4600 and (3) during recent time (CE 2015) – cal BP ~260. The first period was conspicuously high during the main dry phase concomitant with high fluxes of organic compounds to the bottom and suboxic-anoxic conditions in the sediments. This period reached a maximum at cal BP ~6700, followed by a continuous increase in moisture levels, low primary productivity and a more oxygenated environment towards the present, being remarkably stronger in the last 2000 years. We suggest that this might be associated with greater El Niño frequencies or similar conditions that increase precipitation, concomitantly with the introduction of oxygenated waters to coastal zones by the propagation of equatorial origin waves.

Keywords: paleoproductivity, paleoredox, trace metals, diatoms, opal, organic carbon, Coquimbo, SE-Pacific

1. Introduction

The northern-central Chilean continental margin (18−30°S) has distinct zones of intense upwelling highly influenced by topographic features (Figueroa and Moffat, 2000). As a result, high primary production (0.5-9.3 g C m^{-2} d^{-1}) are developed off Iquique (21°S), Antofagasta (23°S) and Coquimbo (30°S) (González et al., 1998; Daneri et al., 2000, Thomas et al., 2001). This productivity takes place close to the coast above the narrow continental shelf, allowing the development of important fisheries and accounting for up to 40% of total annual catches (Escribano et al., 2004 and references therein).

This high productivity maintains a zone of low dissolved oxygen content along the Chilean margin, reinforcing the oxygen minimum zone (OMZ) that develops along the North and South Pacific Ocean, where their intensity, thickness, and temporal stability vary as a function of latitude (Helly and Levin, 2004, Ulloa et al., 2012). To the north (e.g. 21°S) and off Peru, the OMZ occurs permanently, can extend into the euphotic zone and, in the case of northern Chile and southern Peru, shows no significant interface with the benthic environment due to the presence of a narrow continental shelf (Helly and Levin, 2004).

Past changes in the productivity and oxygenation of bottom waters at different timescales have been evidenced in the SE Pacific through sedimentary records that cover from the Last Glacial Maximum (cal BP 22,000 −18,000) to the present. Different climate-ocean drivers have been proposed to account for these changes. For instance, latitudinal movements of the Southern Westerlies Winds (SWW) and the Antarctic Circumpolar Current (ACC) have been suggested as potential mechanisms (Hebbeln et al., 2002; Lamy et al., 2001; 2002; 2010). In addition, changes in the intensity and position of the Southeast Pacific Subtropical Anticyclone (SPSA) from seasonal, to interdecadal timescale have effects on wind stress and water mass circulation (Ancapichún and Garcés-Vargas, 2015), and therefore past variability in the SPSA has been used to explain changes in paleoceanographic features of the SE Pacific such as the intensity of upwelling, and circulation patterns responsible for the nutrient supply (Marchant et al., 1999; Hebbeln et al., 2002; Dezileau et al., 2004; Romero et al., 2006; Mohtadi et al., 2008; Gutiérrez et al., 2009; Saavedra-Pellitero et al., 2011; Muñoz et al., 2012). Past climate-upwelling fluctuations at millennial timescales has also been linked to the austral insolation, which influence Antarctic sea ice extent and the Hadley cell, this latter an important forcing to the latitudinal cycle of the ITCZ (Intertropical

Convergence Zone; Kaiser et al., 2008 and reference there in). This variability produces humid and arid conditions along the SE Pacific where the intensity of wind has a key role for the upwelling and hence productivity. On top of all this, an important driver of modern ocean-atmosphere conditions in the South East Pacific is the El Nino/Southern Oscillation (ENSO), which has a major impact on modern marine productivity (Escribano et al., 2002). Paleo-ENSO reconstructions indicate attenuated ENSO events before the mid-Holocene (last 5000 years) and increasing from this period towards the present (Marchant et al., 1999;; Koutavas et al., 2006; Vargas et al., 2006), consistent with paleoceanographic and paleoclimate interpretations (Rodbell et al., 1999; Rein et al., 2005). Heavy rainfall episodes in the south East Pacific normally occur during strong El Niño conditions (Montecinos and Aceituno, 2003), increasing the river flux and producing flood debris (Garreaud and Rutllant, 1996). These episodes have been recorded in sedimentary records off northern Chile and southern Peru, establishing a teleconnection which has operated since the mid-Holocene, and identifying the modern manifestation of El Niño starting at ~5000 cal BP (Vargas et al., 2006).

The effect of climate variations on primary productivity and biogeochemical cycles could have different responses. For instance, the increase in land-sea thermal contrast in North-Central Chile enhances upwelling and with it, exported production (Vargas et al., 2007). Other evidence, however, suggest that the intrusion of warmer oligotrophic water reduce primary productivity, as observed during the 97-98 ENSO event (Iriarte and Gozález, 2004). Furthermore, in South central Chile (36°S) the oxygenation of bottoms was clearly detected during the 97-98 El Niño event, changing the geochemical conditions of surface sediments and macrofauna composition. These disturbances may extend considerably to the south, with implications persistent for many years and impact the sedimentary records of several proxies (Sellanes et al., 2007; Gutiérrez et al., 2006). Our work focuses on the past variations of the environmental conditions and marine productivity in sedimentary records from a transitional semi-arid ecosystem of Central Chilean coast (30°S), an area highly susceptible to oceanographic and climatic forcing. The study area (Fig. 1) provides an adequate platform to observe environmental variability at different time scales. We were able to identify wet/dry intervals, periods with high/low primary production, and changes in redox conditions at bottoms through inorganic (trace metals) and organic proxies.

2. Study area

The Coquimbo area (29-30°S), in the southern limit of the northern-central Chilean continental margin, constitutes a border area between the most arid zones of northern Chile (Atacama Desert) and the more mesic Mediterranean climate of central Chile (Montecinos et al., 2015). Here, the shelf is narrow and several small bays trace the coast line.

The Tongoy and Guanaqueros bays are located at the southern edge of a broad embayment between small islands in the north (29°S; Choros, Damas and Chañaral) and Lengua de Vaca Point in the south (30°S) (Fig. 1), protected from predominant southerly winds. Tongoy Bay is a narrow marine basin (10 km at its maximum width) with a maximum depth of ~100 m. To the northeast lies Guanaqueros Bay, a smaller and shallower basin. Favorable winds throughout the year promote an important upwelling center at Lengua de Vaca Point, developing high biomass along a narrow coastal area (Moraga-Opazo et al., 2011), and reaching maximum concentrations of ~20 mg m^{-3} (Torres et al., 2009). At the shallow waters of Tongoy Bay, the high primary productivity results in high TOC in the water column allowing the deposition of fine material on the bottom; TOC increases concurrently with the periods of low oxygen conditions (Fig. 3; Muñoz et al., unpublished data). Recent oceanographic studies indicate that the low dissolved oxygen water intrusions from the shelf (Fig. 2) seems to be related to sea level decreases resulting from local wind annual cycles at a regional meso-scale (Gallardo et al., 2017). The spatial and temporal variability of these processes are still under study.

Sedimentological studies are scarce in the northern-central Chilean shelf. A few technical reports indicate that sediments between 27°S and 30°S are composed of very fine sand and silt with relatively low organic carbon content (<3 and ~5%), except at very limited coastal areas where organic material accounts for around ~16% (Muñoz, unpublished data; FIP2005-61 Report, www.fip.cl). Coastal weathering is the main source of continental input due to scarce river flows and little rainfall in the zone (0.5 to ~20 mm yr^{-1}; https://es.climate-data.org/location/940/, Fig.1). Freshwater discharges are represented by creeks, which receive the drainage of the coastal range forming wetland areas in the coast and even small estuaries, as Pachingo located south of Tongoy (Fig. 1). These basins cover ~300 and 487 km^2, respectively. The water volume in the estuaries is maintained by the influx of seawater mixed with groundwater supply. No surface flux to the sea is observed. Therefore, freshwater discharge occurs only during high rainfall periods in the coastal zone (DGA, 2011), which normally takes place during El Niño years when higher runoff has been recorded in the area during austral winter time (Valle-Levinson et al., 2000; Garreaud et al., 2009). In this scenario marine sediments are often highly influenced by primary production in the water column, and therefore sedimentary records can reveal past variability in primary production and the oceanographic conditions over the shelf, which ultimately respond to major atmospheric patterns.

3. Materials and methods

3.1. Sampling

Sediment cores were retrieved from two bays in the Coquimbo region: Bahía Guanaqueros (core BGGC5; 30°09' S, 71°26' W; 89 m water depth) and Bahía Tongoy (core BTGC8; 30°14' S, 71°36' W; 85 m water depth) (Fig. 1.), using a gravity corer (KC-Denmark) in May 2015, on board the L/C Stella Maris II owned by the Universidad Católica del Norte. The length of the cores was 126 cm for BGGC5 and 98 cm for BTGC8. Both cores were cut along the main axis and a general visual characterization was done. Different textures and color layers were identified using the Munsell color chart.

Subsequently, the cores were sliced into 1-cm sections and subsamples were separated for grain size measurements, magnetic susceptibility, trace elements, biogenic opal, C and N stable isotope signatures ($\delta^{13}C$, $\delta^{15}N$), and TOC analyses. The samples were first kept frozen (–20° C) and then freeze-dried before laboratory analyses.

The magnetic signal indicates the concentrations and compositions of magnetic minerals and is usually used combined with others detrital proxies such as grain size to establish changes in sedimentary processes closely controlled by climatic conditions. We considered redox trace elements measurements that respond to local hypoxia (U, Mo and Re) as well as nutrient-type elements, which follow the organic fluxes to the sediments (Ba, Ni Cu, P). Additionally, we measured Fe and Mn which play a key role in adsorption-desorption and scavenging processes of dissolved elements in the bottom water and sediments. We also measured Ca, K and Pb used to assess terrigenous inputs by coastal erosion, weathering and eolian transport, which is also true for Fe and Mn. Ca accumulation within the sediments depends, in turn, on the carbonate productivity and dissolution, which has been used as a paleoproductivity proxy (Paytan, 2008; Govin et al., 2012). We use Al as a normalizing parameter for enrichment/depletion of elements due to its conservative behavior. The crustal contribution and the elements are presented as metal/Al ratios. The authigenic enrichment factor of elements was estimated according to: EF = $(Me/Al)_{sample}$ / $(Me/Al)_{detrital}$; where $(Me/Al)_{sample}$ is the bulk sample metal (Me) concentration normalized to Al content and the denomination “detrital” indicates a lithogenic background (Böhning et al., 2009). Detrital concentrations ($[Me]_{detrital}$ and $[Al]_{detrital}$) were established considering the local TM abundance, which is more accurate than using mean Earth crust values (Van der Weijden, 2002). We used the average of element concentrations at the surface sediments (0−3 cm) of Pachingo wetland (Table 1).

Diatoms and siliceous microfossils were identified and counted. Diatoms assemblages along with biogenic opal content constitute our proxies of siliceous export production. Pollen grains were also identified and counted, and used to identify wet and dry environmental conditions based on the climate relationship of the main vegetation formation in north-central Chile. TOC and stable isotopes of organic matter were used to identify the variability of organic fluxes to the bottom and establish biogeocheemical changes in the organic matter remineralization.

3.2, Geochronology (^{210}Pb and ^{14}C)

^{210}Pb activities were quantified through alpha spectrometry of its daughter ^{210}Po in secular equilibrium with ^{210}Pb, using ^{209}Po as a yield tracer (Flynn, 1968). The chemical procedure considered a total digestion of the sediment samples and then autoplated onto silver disks at ~75°C for 3 three hours in the presence of ascorbic acid. The ^{210}Po activity was counted in a CANBERRA QUAD alpha spectrometer, model 7404, until the desired counting statistics was achieved (4−10% 1σ errors) in the Chemical Oceanography Laboratory of Universidad de Concepción. ^{210}Po activity –assumed to be in secular equilibrium with ^{210}Pb– was calculated using the ratio between natural radionuclide and the tracer, which is multiplied by the activity of the tracer at the time of plating. The period elapsed between plating and counting produces ^{210}Po decay (half-life: 138 days) and between sampling and plating ^{210}Pb decay (half-life: 22.3 yr); counting was corrected to these elapsed times even when there was a short time period between the collection date and the time of sample analysis (less than one year). Ages were estimated using the inventories of the activities in excess ($^{210}Pb_{xs}$, unsupported), based on the Constant Rate of Supply Model (CRS, Appleby and Oldfield, 1978). Unsupported activities were determined as the difference between ^{210}Pb and ^{226}Ra activities measured in some sediment column intervals. ^{226}Ra was measured with a gamma spectrometry at the Laboratoire Géosciences of the Université de Montpellier (France). Standard deviations (SD) of the ^{210}Pb inventories were estimated propagating counting uncertainties (Bevington and Robinson, 1992) (Table S1, supplementary data). Radiocarbon measurements were performed on a mix of planktonic foraminifera species in core BGGC5 whereas the benthic foraminifera species *Bolivina plicata* was selected for core BTGC8 (Table 2). Freeze-dried sediment was washed over a 63 µm mesh-size sieve and dried after washing at 50°C. At least 2 mg of mixed planktonic foraminifera were picked from the 125−250 µm fraction. The samples were submitted to the National Ocean Sciences AMS Facility (NOSAMS) of the Woods Hole Oceanographic Institution (WHOI). The Fraction Modern (Fm) was corrected by the $\delta^{13}C$ value, and ages were calculated using 5568 (yrs) as the half-life of radiocarbon. The time scale was obtained according to the best fit of $^{210}Pb_{xs}$ curves and ^{14}C points, using the CLAM 2.2 software and Marine curve 13C (Reimer et al, 2013), and considering a reservoir of 146 ±25 years, established for Coquimbo coastal margin (Carré et al., 2016) (Fig. 4).

3.3. Geophysical characterization

Magnetic susceptibility ($SIx10^{-8}$) was measured with a Bartington Susceptibility Meter MS2E in the Sedimentology Laboratory at Centro Eula, Universidad de Concepción. Mean values from three measurements were calculated for each sample.
Grain size was determined using a Mastersizer 2000 laser particle analyzer, coupled to a Hydro 2000−G Malvern in the Sedimentology Laboratory of Universidad de Chile. Skewness, sorting and kurtosis were evaluated using the GRADISTAT statistical software (Blott and Pye, 2001), which includes all particle size spectra.

3.4. Trace elements analysis

Trace element analyses were performed by ICP-MS (Inductively Coupled Plasma-Mass Spectrometry) and carried out at Université de Montpellier 2, France (OSU OREME/AETE regional facilities), using an Agilent 7700x. About 50 mg of samples and geochemical reference materials (UBN, BEN and MAG1) were dissolved twice through the conventional digestion method using a concentrated HF-HNO_3-$HClO_4$ mix (1:1:0.1) in Savillex screw-top Teflon beakers at 120°C, on a hot plate during 48h. Following digestion, the samples were subjected to three evaporation steps in order to remove fluorine. Shortly before analysis, samples were dissolved in 2 ml of concentrated HNO_3 and transferred to 20 ml polypropylene bottles. Final sample preparation was undertaken by dilution with ultrapure water to a sample-solution weight ratio of 1: 4000-5000 and the addition of a known weight of internal standard solution consisting of 1 ppb of In and Bi. Internal standardization used ultra-pure solution enriched in In and Bi, both elements whose natural abundances in geological samples do not contribute significantly to the added internal standard. This is used to deconvolve mass-dependent sensitivity variations of both matrix and instrumental origin, occurring during the course of an analytical session.

Sample introduction uses a peristaltic pump, a micro-nebulizer and a cooled double-pass Scott type spray chamber. The uptake time (typically 45 s) is set to facilitate stable analyte signals prior to a 120 seconds analysis for each sample. Elements with an atomic mass lower than 80 were analyzed in collision mode using He; heavier elements were analyzed in no-gas mode. A wash out procedure consisting of 60 seconds with HNO_3 10% and 120 seconds with 2% HNO_3 has been found appropriate to achieve instrument blank level. The total time for analysis of a single sample solution is *c.* 3 minutes. Mean concentrations for the analyzed samples were determined by external calibrations prepared daily from multi- and mono-elemental solutions, with concentrations in the range of 0.05−10 ppb for trace elements and of 1−10 ppm for major elements (Ca, K). Polyatomic interferences were controlled by running the machine at an oxide production level <1%. Typical analytical precisions attained by this technique are generally between 1% and 3%, relative standard deviation. Accuracy has been assessed with an analysis of international reference materials and results show agreement generally better than ±5% with reference values.

3.5. TOC and stable isotopes

TOC and stable isotope ($\delta^{15}N$ and $\delta^{13}C$) analyses were performed at the Institut für Geographie, Friedrich Alexander Universität (FAU) Erlangen-Nürnberg, Germany. Dry material was placed into tin and silver capsules for N and C analyses respectively, and combusted at 1060° C in a continuous helium flow in an elemental analyzer (NC2500, Carlo Erba), in the presence of chromium oxide and silvered cobalt oxide. The resulting gases, were passed over copper wires at 650° C to reduce nitrogen and excess oxygen. Thereafter, water vapor was trapped with $Mg(ClO_4)_2$ and the remaining gases (N_2 and CO_2) were separated in a gas chromatography column at 45° C. N_2 and CO_2 were passed successively via a ConFloII interface into the isotope-ratio-mass spectrometer

(Delta Plus, Thermo-Finnigan) and isotopically analyzed. Carbon and nitrogen contents were determined from the peak-area-versus-sample-weight ratio of each individual sample and calibrated with the elemental standards cyclohexanone-2,4-dinitrophenylhydrazone ($C_{12}H_{14}N_4O_4$) and atropine ($C_{17}H_{23}NO_3$) (Thermo Quest). A laboratory-internal organic standard (Peptone) with known isotopic composition was used for final isotopic calibrations. Stable isotope ratios are reported in the δ notation as the deviation relative to international standards (Vienna Pee Dee Belemnite for $\delta^{13}C$ and atmospheric N_2 for $\delta^{15}N$), so $\delta^{13}C$ or $\delta^{15}N = [(R\ sample/R\ standard) - 1] \times 10^3$, where R is $^{13}C/^{12}C$ or $^{15}N/^{14}N$, respectively. Typical precision of the analyses was ±0.1‰ for $\delta^{15}N$ and $\delta^{13}C$.

3.6. Biogenic opal

Biogenic opal was estimated following the procedure described by Mortlock and Froelich (1989) with a slight modification, which consists in extracting 50 mg of sediment with 1 M NaOH (instead of 2 M Na_2CO_3) at 85°C for 5 hours. Extraction and analysis by molybdate-blue spectrophotometry (Hansen and Koroleff, 1999) were conducted at the laboratories of Marine Organic Geochemistry and Paleoceanography, University of Concepción, Chile. Values are expressed as biogenic opal by multiplying the Si (%) by 2.4 (Mortlock and Froelich, 1989). Analytical precision was ± 0.5%. Accumulation rates were determined based on sediment mass accumulation rates and amount of opal at each core section in %.

3.7. Diatoms and siliceous microfossils

Smear slides for qualitative abundances of siliceous microfossils were carried out every centimeter following the Ocean Drilling Program (ODP) protocol described by Mazzullo et al. (1988.) To determine the quantitative abundance of siliceous microfossils (diatoms, silicoflagellates, sponge spicules, crysophyts and phytoliths), ~ 0.5 g of freeze-dried sediment was treated according to Schrader and Gersonde (1978). Samples were chosen every ~4, 8 and 12 cm for BGGC5 and at an average of 6 cm for BTGC8. Permanent slides were prepared by placing a defined sample volume (0.2 ml) onto microscope slides that were then air-dried and mounted with Naphrax mounting medium (refraction index =1.3). Siliceous microfossils were identified and counted under an Olympus CX31 microscope with phase contrast. 1/5 of the slides were counted at 400X for siliceous microfossils and one transect at 1000x was counted for *Chaetoceros* resting spores. Two slides per sample were counted; the estimated counting error was 15%. Total diatom abundances are given in valves g^{-1} of dry sediments.

3.8. Pollen

Sample preparation for pollen analysis was conducted following the standard methodology for sediment samples (Faegri and Iversen, 1989), which includes deflocculating with 10% KOH, carbonate dissolution with a 5% HCl treatment, silica dissolution with 30% HF, and cellulose removal *via* acetolysis reactions. Samples were mounted with liquid glycerol and sealed permanently with paraffin wax. Pollen identification was conducted under a stereomicroscope at 400 fold magnification with the assistance of the Heusser (1971) pollen catalogue. A total of 100-250 terrestrial pollen grains were counted on each sample depending on their abundance. Pollen percentage for each taxon was calculated from the total sum of terrestrial pollen. The percentage of aquatic pollen and fern spores was calculated based on the total terrestrial sum plus their respective group. Pollen percentage diagrams were generated using the Tilia software (E. Grimm, Illinois State Museum, Springfield, IL. USA). The diagram was divided into "zones" based on the identification of the most important changes in pollen percentage and assisted by a cluster ordination (CONISS) performed by the same software.

We further summarize pollen-based precipitation trends by calculating a Pollen Moisture Index (PMI), which is defined as the normalized ratio between Euphorbiaceae (wet coastal scrubland) and Chenopodiaceae (arid scrubland). Thus, positive (negative) values of this index indicate the relative expansion (reduction) of coastal scrubland under relatively wetter (drier) conditions.

4. Results

4.1. Geochronology

$^{210}Pb_{xs}$ (unsupported activity) was obtained from the surface down to 8 cm depth in the two cores, with an age of ~ AD 1860 at 7 cm in both of them (Table S1). Greater surface activities were obtained for core BGGC5 (13.48 ± 0.41 dpm g^{-1}) compared to core BTGC8 (5.80 ± 0.19 dpm g^{-1}), showing an exponential decay with depth (Fig. 4). A recent sedimentation rate of 0.11±0.01 cm yr^{-1} was estimated.

The age model provided a maximum age of cal BP 8469 for core BGGC5, and cal BP 8199 for core BTGC8 (Fig. 4). A mean sedimentation rate of 0.02 cm yr^{-1} was estimated for core BGGC5, with a period of relative low values (0.01 cm yr^{-1}) between cal BP 4000 and 6000. For BTGC8, sedimentation rates were less variable and around 0.013 cm yr^{-1} in the entire core. An age reservoir estimation following the methodology of Sabatier et al. (2010) resulting in, 441 and 442 years for BGGC5 and BTGC8 cores, respectively (Table 3). These values were close to global marine reservoir and higher than other estimations along Chilean margin at shallower depths (146 ± 25 years at < 30 water depth; Carré et al., 2016; Merino-Campos et al., 2018). Our cores sites are deeper (~90 m water depth) receiving the influence of upwelled water from Lengua de Vaca Point, which could explain such differences. However, moderated differences were observed between models using these different reservoir values. Our estimations were based only on two pre-bomb values established with 210Pb measured in sediments and 14C in foraminifers, therefore the value estimated by Carré et al. (2016) was used for the age modeling; but this situation deserve attention and tested with a larger set of data

4.2. Geophysical characterization

The sediments retrieved from the bays showed fine grains in the range of very fine sand and silt in the southern areas. There, the grain size distribution was mainly unimodal, very leptokurtic, better sorted and skewed to fine grain when compared to sediments from the northern areas. Sediment cores obtained from the northern areas were sandy (coarse sand and gravel), with abundant calcareous debris. Longer cores of soft sediment were retrieved at the southern areas (BGGC5 and BTGC8), where the silty component varied between 40 % and 60 % (Fig. 1 and 5a,b). The clay component was very low at both cores (<2%). The sediment’s color ranged from very dark grayish brown to dark olive brown (2.5Y 3/3−3/2) at Guanaqueros Bay (BGGC5) and from dark olive gray to olive gray (5Y 3/2−4/2) at Tongoy Bay (BTGC8). Visible macro-remains (snails and fish vertebrae) were found and weak laminations were identified at both cores. The magnetic susceptibility showed higher values close to the surface, up to 127 SI $x10^{-8}$ at BGGC5 and relative lower values (85 SI $x10^{-8}$) at BTGC8. At greater depths, however, the values were very constant, around 5−8 $x10^{-8}$ SI at BGGC5 core and around 12−20 $x10^{-8}$ SI at BTGC8 core. In both cores, susceptibility increases substantially after cal BP 13 (Figs. 5a, 5b). Lower bulk densities were estimated at the core BGGC5 (0.7−0.9 g cm^{-3}) compared to the core BTGC8 (>1 g cm^{-3}) (Fig. 5a, 5b). In accordance with this, the mean grain size was 60−80 µm at Guanaqueros Bay (BTGC8), compared to 50−60 µm at Tongoy Bay (BGGC5). Both cores were negatively skewed, with values of -1 to -1.2 at BGGC5, and -1 to -2.5 at BTGC8. Minor increases towards coarser grain size were observed in the last 2000 years, especially at Tongoy Bay (BTGC8). In both cases, grain size distributions were strongly leptokurtic. Ca/Fe ratio also diminished in time, except at core BTGC8 where it was only observed during the last ~2300 years. The diminishing of the Ca/Fe ratio is due to a decrease in Ca content mainly but also because of a slight increase in Fe within the sediments (Figs. 6a, 6b).

4.3. Biogenic components

4.3.1. Siliceous microfossils and biogenic opal

Total diatom abundance fluctuated between 5.52 $x10^5$ and 4.48 $x10^7$ valves g^{-1} in core BGGC5. Total diatom abundance showed a good correlation with biogenic opal content at BGGC5 (R^2 =0.52, P<0.5), with the highest values from 72−74 cm to the bottom of the core, corresponding to cal BC 3390−3790. In contrast, diatom abundance and biogenic opal were much lower in core BTGC8 (< 2 $\times10^5$ valves g^{-1} and <3%, respectively). Here, the siliceous assemblage was almost completely conformed by *Chaetoceros* resting spores (RS) (Fig. 7).

A total of 135 and 8 diatom taxa were identified in cores BGGC5 and BTGC8 respectively, where the core BTGC8 registered very low abundances of diatoms. In general, diatoms were the most important assemblage of siliceous microfossils (96%), followed by sponge spicules (3%). The contribution of phytoliths and chrysophyte cysts was less than 2% in core BGGC5. *Chaetoceros* (RS) dominated the diatom assemblage (~90%; Fig. 7), and included the species *C. radicans*, *C. cinctus*, *C. constrictus*, *C. vanheurckii*, *C. coronatus*, *C. diadema*, and *C. debilis*. Other species recorded of upwelling group (mainly in core BGGC5) were: *Skeletonema japonicum*, and *Thalassionema nitzschioides* var. *nitzschioides* (Table S2). Freshwater diatoms (*Diploneis papula, Cymbella tumida, Fragilaria capucina, Diatoma elongatum)* and non-planktonic diatoms (*Cocconeis scutellum, C. costata and Gramatophora angulosa*) accounted for ~0.1−5%; while the group of coastal planktonic diatoms accounted for ~0.3− 6% of the total assemblage. The main planktonic diatoms were (*Rhizosolenia imbricata*, and *Thalassiosira eccentrica*). Oceanic-warm diatoms (*Roperia tesselata, Th. nitzschioides var inflatula)* and the tycoplanktonic diatom group were rare with less than 1%.

4.3.2. TOC and stable isotopes distribution

Consistent with opal and diatoms, core BGGC5 showed higher values of TOC (between 2 % and 5 %) compared with less than ~1.5 % in core BTGC8 (Fig. 5a,b). Furthermore, $\delta^{13}C$ was slightly higher at core BTGC8 (-20 ‰ to -21 ‰) compared with core BGGC5 (-21 ‰ to -22 ‰), the former also showing slightly increased values of $\delta^{15}N$ from the deeper sections to the surface of the core (<7 ‰ to >10 ‰). This increase was less evident at core BGGC5, with values of ~9 ‰ at depth to >10 ‰ on the surface (Fig. 5a,b). Diminishing TOC contents was related to slightly higher $\delta^{13}C$ values (~ -20 ‰) in both cores.

4.3.3. Pollen record

Initial surveys on core BTGC8 (Tongoy Bay) revealed extremely low pollen abundances which hampered further palynology work. A comprehensive pollen analysis was only conducted for core BGGC5 (Guanaqueros Bay). The pollen record of core BGGC5 consisted of 29 samples shown in Figure 8. The record was divided in five general zones following visual observation of changes in the main pollen types and also assisted by the cluster analysis CONISS.

Zone BG-1 (cal BP 8450 – 8000): This zone is dominated by the herbaceous taxa Chenopodiaceae, *Leucheria*-type, Asteraceae subfamily (subf.) Asteroideae, Apiaceae with overall high values of the wetland genus *Typha* spp.

Zone BG-2 (cal BP 8000 – 6850): This zone is also dominated by Chenopodiaceae, *Leucheria*-type and Asteraceae subf. Asteroideae. In addition, other non-arboreal elements such as *Ambrosia*-type, Poaceae, Brassicaceae and *Chorizanthe* spp. expand all considerably.

Zone BG-3 (cal BP 6850 –3750): This zone is marked by a steady decline in Chenopodiaceae and *Leucheria*-type, and by the expansion of several other herbaceous elements, such as Euphorbiaceae, *Baccharis*-type and Brassicaceae.

Zone BG-4 (cal BP 3750 – 250): This zone is mostly dominated by Ast. subf. Asteroideae, and marked by the decline of Chenopodiaceae and *Leucheria*-type. Other coastal taxa such as Euphorbiaceae, *Baccharis*-type, Asteraceae subf. Chichorioideae, *Quillaja saponaria*, Brassicaceae and *Salix* spp. also expand in this zone.

Zone BG-5 (cal BP 250 – -60): The upper portion of the record is dominated by Asteraceae subf. Asteroideae and Poaceae, and marked by increments of Geraniaceae, Asteraceae subf. Mutisieae, Myrtaceae and *Q. saponaria*. Additionally, this zone includes introduced pollen types such as *Rumex* spp. and *Pinus* spp. The latter is not shown in the diagram of Figure 8 because its abundance was minimal.
Overall, the most distinctive trend revealed in core BGGC-5 is a long-term decrease in Chenopodiaceae and increments in Euphorbiaceae and Asteraceae subf. Asteroideae. Along with these changes, a later expansion of several other pollen representatives of the coastal shrubland vegetation started at around cal BP 6850.

4.4. Trace element distributions

Trace element distributions are shown in figures 6a and 6b for Guanaqueros (BGGC5) and Tongoy Bays (BTGC8), respectively. Trace metals sensitive to the presence of oxygen (U, Re, Mo) showed increasing metal/Al ratios from the base of the core (cal BP ~8400) until cal BP 6700 in core BGGC5. After this maximum, ratios presented a slight increase towards cal BP 2000 close to the beginning of the recent era, followed by a sharp decrease until present. Similarly, the metal ratios in the core BTGC8 increase over time, yet the maximum was observed at cal BP 1100. The exception of this trend was Mo which exhibited maximum values until cal BC 6700 and then a steady decrease towards the present. Additionally, metal/Al values were higher at core BGGC5. Iron displayed a clear increase around cal BP 4100 − 3600 at both cores. Manganese did not show any clear trend.
A second element group (metal/Al ratios), including Cd, Ni and P (related to primary productivity and organic fluxes), showed a similar pattern than Mo/Al towards the bottom of core BGGC5, i.e. the highest values around cal BP 6700 and a constant reduction towards the present. A third group, consisting of Ba, P and Ca, exhibited a less clear pattern. The Cd/Al and Ni/Al ratios in core BTGC8 showed only slightly decreasing values, and the maximum values were very low compared to the BGGC5 core. The same pattern is observed for other elements. Metal/Al ratios for Ba, Ca and P were lower and presented a long-term decreasing pattern towards the present.
An exception to the previously described patterns was Cu/Al, which peaked at cal BP 4100 and showed a conspicuous increase in the past ~150 years. This was also observed at core BTGC8, but with lower concentrations than at core BGGC5.

5. Discussion

5.1. Sedimentary composition of the cores: terrestrial *versus* biogenic inputs

The sediments in the southern zones of the bays constitute a sink of fine particles transported from northern areas and the shelf (Fig. 5a, 5b), responding to the water circulation in the Guanaqueros and Coquimbo Bays described as bipolar, i.e. two counter-rotating gyres which are counterclockwise to the north and clockwise to the south (Valle-Levinson and Moraga, 2006). This is the result of the wind and a coastline shape delimited by two prominent points to the north and south. In the case of Tongoy Bay (the southernmost bay of the system), circulation shows a different pattern due to its northern direction compared to Guanaqueros Bay, which opens to the west. The cyclonic recirculation in Tongoy Bay seems to be part of a gyre larger than the Bay's circulation (Moraga et al., 2011). This could explain differences in sediment particle distribution and composition between the bays. At Tongoy Bay, there are less organic carbon accumulation (< 2 %), siliceous microfossils and pollen (Figs. 5, 7 and 8). Similarly, in Guanaqueros Bay TOC contents are only slightly higher (> 2 %), especially before cal BP 6000 (~ 4 %). However, sediments there contain enough microfossils to establish differences in primary productivity periods and also provide a pollen record evidencing the prevailing environmental conditions.

The stable isotopes measured in the study area were in the range of marine sedimentary particles for southern oceans at low and mid latitudes ($\delta^{13}C$; -20 ‰ – -24 ‰; Williams 1970; Rau et al., 1989; Ogrinc et. al. 2005), and slightly lower than the TOC composition at the water column (-18 ‰, Fig. 3). This suggests that the organic particles that settle on the bottom are a more refractory material (C/N: 9−11), remineralized during particle transportation and sedimentation. This results in lighter isotopic compositions, especially at core BTGC8. Furthermore, the $\delta^{15}N$ and $\delta^{13}C$ of settled particles are more negative at surface sediments due to a preferential degradation of molecules rich in ^{13}C and ^{15}N, resulting in more negative values and higher C/N ratios at sediments than in suspended particles (Fig. 3, 5a, 5b). However, this is also due to the stronger diagenetic reactions observed near the bottom layer (Nakanishi and Minagawa, 2003),. Thus, these sediments are composed by winnowed particles transported by water circulating over the shelf, and the isotopic variations should not establish clearly the contribution of terrestrial inputs.

Otherwise, the isotopic composition of upwelled NO_3 (De Pol-Holz et al., 2007) could influence the variability of $\delta^{15}N$. Values for $\delta^{15}N$ at northern and central Chile are in the range of those measured at BGGC5 core (~11‰; Hebbeln et al., 2000, De Pol-Holz et al., 2007), resulting by the isotopic fractionation of NO_3 during nitrate reduction within OMZ leaving a remnant NO_3 enriched in ^{15}N (Sigman et al., 2009; Ganeshram et al., 2000 and references therein). In this case, the BGGC5 core sediments represent the effect of the nutrient supply by the upwelling and the influence of the OMZ over the shelf resulting in $\delta^{15}N$ of 9 − 10‰. At BTGC8 sediment core, lower values (<8‰) at greater depths within the core should represent the mixing with light terrestrial organic material (Sweeney and Kaplan, 1980), due to the nearest position of a permanent small wetland at southern site of Tongoy Bay. Pachingo wetland material showed $\delta^{15}N$ of 1 − 8‰ (Muñoz et al., data will be published elsewhere) in the range of sedimentary environments influenced by terrestrial runoff (Sigman et al., 2009). At most of the cases, lower TOC is correspondingly with lighter $\delta^{15}N$ values, and also with the highest C/N ratios (Fig. 5b).

Magnetic susceptibility (MS) measurements revealed lower values throughout both cores (BGGC5: 5 – 8 $x10^{-8}$ SI; BTGC8: 12 – 20 $x10^{-8}$ SI), except at dates of the last ~100 years (CE 1800), when it increases substantially to values similar to those observed in the Pachingo wetland (40 – ~200 $x10^{-8}$ SI; unpublished data) on the southern side of Tongoy Bay. Magnetite has strong response to magnetic fields and its concentration is considered proportional to magnetic susceptibility (Dearing, 1999). Additionally, mineral post-depositional transformations (alteration of magnetite minerals) and dilution by biogenic components (carbonates, silicates) should also be relevant in the MS intensity in zones with high organic accumulation rates (Hatfield and Stoner, 2013). However, this is not expected to be the case for our cores and the MS should be mainly accounting for the source of the particles. The highest MS measurements on surface sediments would indicate a greater contribution of terrestrial material. The area is surrounded by several creeks that are only active during major flooding events, with greater impacts on Tongoy Bay compared to Guanaqueros Bay. An important increment in the contribution of terrestrial material has occurred in Tongoy Bay in recent times (Ortega et al., in review), which is diluting organic proxy records and increasing the grain size. Our records indicate a slight increase in mean grain size at both bays, supported also by a slight decrease in Ca/Fe ratio indicating more Fe input from continental erosion (Fig. 5a, 5b).

Recent information indicates that during the intensification of southern winds the upwelling develops a nutrient-rich and low-oxygen flow within the bay's southern areas (Gallardo et al., 2017), which promotes phytoplankton blooms and low oxygen events. Decreasing concentrations of Ca from the deepest part of both cores to the surface was interpreted as decreasing primary productivity (Keshav and Achyuthan, 2015; Sun et al., 2016), but higher concentrations were measured in core BGGC5 compared with core BTGC8, where more terrestrial influence is being suggested. The slight increase of K/Ca ratio in time, from bottom to the surface, should also be interpreted as a slight increase in continental input, since K is related to siliciclastic material from coastal erosion, fluvial and groundwater inputs. However, the variation of Ca was larger (Fig.6a, 6b), resulting in higher K/Ca ratios at the surface. This indicating that the continental input has not changed much in time but rather the primary productivity has decreased (Fig. 5a, 5b).

5.2. Temporal variability of proxies for primary productivity

Several elements participating in phytoplankton growth are useful to interpret variations in primary productivity in time, as they are preserved in the sediments under suboxic-anoxic conditions. This produces enrichment over crustal abundance, which distinguishes them from continental inputs. The presence of free dissolved sulfides produced by sulfate reduction reactions in the diagenesis of organic matter allows for theprecipitation of metals onthe pore water (Calvert and Pedersen, 1993; Morse and Luther, 1999). At the same time, organic matter remineralization releases ions to the pore water where they could form organic complexes and insoluble metal sulfides. Conversely, they could be incorporated into pyrite as Cd, Ni and Cu, showing different degrees of trace metal pyritization (Huerta-Diaz and Morse, 1992). Ca, Sr, Cd and Ni profiles suggest a lower proportion of organic deposition in time (Fig. 6a, 6b), consistent with the slight reduction of TOC content observed in the sediments (Figs. 5a, 5b), and concomitantly with other elements related to organic fluxes to the bottom and primary productivity. In the case of Ba, it is actively incorporated into phytoplankton biomass or adsorbed onto Fe oxyhydroxides, increasing the Ba flux towards the sediments, where it is also released during organic matter diagenesis. Ba is precipitating in microenvironments where Ba-sulfate reaches supersaturation

(Tribovillard et al., 2006 and references therein), but it is dissolved in suboxic-anoxic environments or where sulfate is significantly depleted (Torres et al., 1996; Dymond et al., 1992). Therefore, it is better preserved in less anoxic environments with moderate productivity, expected to be the case of our study site (Gross Primary Productivity =0.35 to 2.9 g C $m^{-1}d^{-1}$; Daneri et al., 2000). Hence, the slight increase of Ba from cal BP 4000 (Fig. 6a) to the present should rather be the response to a less anoxic environment than to an increase in primary productivity. This is consistent with the reduction in TOC and other nutrient-type elements (Ni, Sr, Ca, Cd), and results in a low negative correlation with TOC (-0.59; Table 4) due to the Ba remobilization in anoxic conditions around cal BP 6700. On the other hand, P distribution showed a trend similar to that of TOC and other elements related to organic fluxes to the bottom (Ni, Cd), although with a lower correlation (~0.6). The accumulation of P depends on the deposition rate of organic P (dead plankton, bones and fish scales) to the bottom, and is actively remineralized during aerobic or anaerobic bacterial activity. Dissolved P diffuses towards the water column where part of it could be adsorbed onto Fe oxides that maintain this element within the sediments. P is buried during a continued sedimentation process and could be released to the pore water under anoxic conditions, when oxides are reduced, creating the environmental conditions for phosphorite and carbonate-fluorapatite precipitation. Normally, this takes place in sites with high sedimentation rates and high organic matter fluxes to the bottom (Filippelli, 1997; Cha et al., 2005), which was not the case for our study area (<0.02 cm yr^{-1}). In spite of this difference, P and TOC showed a decreasing trend towards the present, suggesting reducing flux of organic matter over time, which was also observed for Ni and Cd distributions. Alternatively, it could be explained by the increased remineralization of the organic material settled on the bottom (Figs. 6a, 6b).

Productivity reconstructions were based on diatom relative abundances and biogenic opal content only in core BGGC5, since core BTGC8 registered valve counts that were too low (<1% in relative diatom abundance). However, at both cores diatom assemblages were represented mainly by *Chaetoceros resting spores*, which are used as upwelling indicators, showing increased concentrations during periods of high productivity and upwelling (Abrantes 1988, Vargas et al., 2004). In addition, *Chaetoceros* resting spores are highly silicified and well preserved in coastal sediments (Blasco et al., 1981). The downcore siliceous productivity based on opal distribution (Fig. 7) distinguished three main periods of increased productivity: (1) >

cal BP 6500, (2) cal BP 2000 – cal BP 4600 and (3) recent time (CE 2015) – cal BP ~260. The mean opal accumulation rate in the second period was 11.8 ± 4.8 g m^2 yr^{-1}, when spicules and minerals (quarz, framboid pyrite) where abundant in smear slides. During the first period, accumulation increased noticeably to ~30.1 ± 14.5 g m^2 yr^{-1}, when the *Chaetoceros* spores were predominant, indicating upwelling intensification and low spicules and minerals were observed in the slides. This is partially consistent with the nutrient–type element distributions. Although the third period was too short, high opal accumulation and high Cd/U ratios could also be observed, which increased toward the present (mean opal value of 32.3 ± 22.4 g m^2 yr^{-1}). Similarly, Cu and Fe also increased in recent times (Fig. 6a), contributing to fertilize the environment and promoting primary productivity. The second period was not clearly identified in terms of metals, except for Fe which shows a conspicuous increment in this period (Fig. 6a). During the first period, all metal proxies showed primary productivity increases before cal BP 6500, as indicated by opal accumulation within the sediments. In anoxic-suboxic environments Cd/U ratios could vary between 0.2 and 2 (Nameroff et al., 2002), the high concentrations of both elements reflect anoxic conditions but their different behavior could result in variable Cd/U ratios in suboxic environments. Here, the Cd and U accumulation on sediments resulted in high Cd/U ratios (>2; Fig. 7) during periods with high opal accumulation in the cores, especially in the first period, and even in core BTGC8; and lower ratios (< 1; Fig. 7) when opal was low, indicating higher variations in the primary productivity in time with moderated changes in oxygen conditions at the bottoms. Opal showed good correlations with Ni and Cd (˜0.70; Table 4; Fig. 6a), all suggesting the relevance of bottom organic fluxes for element accumulation within the sediments, and establishing a clear period of higher primary productivity around cal BP 6500, when lowest oxygen conditions prevailed (Fig. 7).

5.3. Temporal variability of proxies for bottom water oxygenation

U, Re and Mo distributions in core BGGC5 indicate that anoxic or suboxic conditions were developed from cal BP 8400 to ~ cal BP 2000. After this period and towards the present, however, a remarkable reduction in their concentration suggests a more oxygenated bottom environment, concurrent with lower organic fluxes to the sediments. The Re profile shows the influence of suboxic waters not necessarily associated with increased organic matter fluxes to the bottom. Since this element is not scavenged by organic particles, its variability is directly related to oxygen changes (Calvert and Pedersen, 2007, and references therein). Additionally, it is strongly enriched above crustal abundance in suboxic conditions (Colodner et al., 1993; Crusius et al 1996), being >10 times in core BGGC5 (Table S3) before cal BP 2000. In the same way, U exhibits a similar pattern, and although organic deposition has an impact on its distribution (Zheng et al., 2002), it also relates to changes in bottom oxygen conditions. This is because its shift from a soluble conservative behavior to non-conservative and insoluble behavior solely depends on the redox potential change that occurs near the Fe(III) reduction zone (Klinkhammer and Palmer, 1991). Molybdenum, which showed high increases at cal BP 6700, also indicates the presence of sulfidic conditions, as shown by the Re distribution highly enriched in anoxic environments (Colodner et al., 1993), and by the reduction of Re(VII) to Re(IV) forming ReO_2 or ReS (Calvert and Pedersen, 2007). Rhenium, U and Mo enrichment are used to decipher the redox condition within the sediments, even in places with high lithogenic input that could obscure the authigenic enrichment of other elements under similar conditions (Crusius et al., 1996). In both places, the concentrations of these elements showed values above the crustal abundance, especially in core BGGC5 (Table S3), with Re and Mo becoming more enriched (>13) than U (~ 5), except at recent time that diminish drastically. This suggests that the presence of anoxic conditions were stronger around cal BP 6300 – 7200 whit a peak at cal BP 6700. The most important enrichment was observed for Cd (> 30) but higher before cal BP 6300 (~147) (Table S3), which could similarly indicate the sulfidic condition within the sediments that allows Cd precipitation. It is also supported by Mo enrichment, since its accumulation within the sediments is highly controlled by sulfide concentrations (Chaillou et al., 2002; Nameroff et al., 2002; Sundby et al., 2004).

Something similar occurs in Tongoy Bay (core BTGC8), but trace metal concentrations are lower for all elements and also for TOC, suggesting that it has limited influence on metal accumulation within the sediments. Thus, these elements suggest anoxic conditions within the sediments in both places around cal BP 6700 − 7200 (Fig. 6a, 6b). After this period, a second maximum but less intense anoxia is observed at the beginning of the recent era (cal BP 2000), continuing with a conspicuous oxygenation until present times. This interpretation based on the distribution of U, Re and Mo complements the observations of nutrient-type elements pointing both to oxygenation changes and to changes in organic fluxes thorough the sediments. A less prominent accumulation of nutrient-type elements (Ni, Cd, Ba, Ca and P) would indicate lower organic material deposition to the sediments but promoting anoxic conditions within the sediments and lower sulfide content with time, which are nevertheless high enough to sustain Mo accumulation until cal BP 2000. After that, a notorious decrease in Re, U and Mo accumulation was observed, suggesting that the oxygenation of the bottom becomes relevant. This could also explain the conspicuous increase of Cu/Al and Fe/Al in recent times due to the presence of oxides (Fig. 6a, 6b). Apparently, a low level of dissolved Cu is maintained by the complexation with organic compounds produced by phytoplankton and Cu adsorption on Fe oxides (Peacock and Sherman, 2004; Vance et al., 2008; Little et al., 2014), with both processes increasing Cu in the particulate phase over surface sediments. At our study sites, Fe and Cu concentrations were higher in surface sediments, probably related to an increase in Fe and Cu availability in the environment (Fig. 6a, 6b). This could be in turn associated with mining activities carried out in the area since the beginning of cal BP 50 (CE 1900's).

At present, the suboxic conditions within the bays result from the influence of adjacent water masses with low oxygen contents, related to the oxygen minimum zone (OMZ) (Fig. 2) centered at ~250 m. Upwelling promotes the intrusion of these waters towards the bays, with strong seasonality. Transition times develop in short periods by changes in wind directions and intensities along the coast. Additionally, oceanic variability along the western coast of South America is influenced by equatorial Kelvin waves on a variety of timescales, from intraseasonal (Shaffer et al.,1997) and seasonal (Pizarro et al., 2002; Ramos et al., 2006) to interannual (Pizarro et al., 2002; Ramos et al., 2008). Coastal-trapped Kelvin waves originating from the equator can propagate along the coast, modify the stability of the regional current system and the pycnocline, and trigger extratropical Rossby waves (Pizarro et al., 2002; Ramos et al., 2006; 2008). This oceanographic feature will generate changes in oxygen content within the bays with major impacts on redox sensitive elements in surface sediments; thus, the increased frequency and intensity of this variability would result in a mean effect which is observed as a gradual change in metal contents in time.

5.4. Climatic interpretations

The present-day climate of the semi-arid region of Chile is largely influenced by the position of the Southeast Pacific Subtropical Anticyclone (SPSA) and latitudinal displacements of the Southern Westerly Winds (SWW). The dynamic of these large-scale atmospheric systems, from seasonal to decadal timescales, control the amount of precipitation that reaches this region. Because the semi-arid region of Chile represent the northernmost area under the influence of the SWW, precipitation is relatively scarce and restricted to the austral winter months when the SPSA and SWW shift northwards, bringing precipitation fronts to the semiarid coast and the interior land (Montecinos and Aceituno, 2003; Quintana and Aceituno, 2012).

In accordance with the modern climatology, paleoenvironmental records from the semiarid region have mostly been interpreted to reflect past variability in the intensity and latitudinal position of the SWW. In this regard, the Holocene period features a series of wet and dry phases resulting from millennial-scale SWW changes (Hebbeln et al., 2002; Lamy et al., 1999; Maldonado and Villagrán, 2002). In particular, pollen records from the southern coastal areas of Coquimbo (32°S) indicate that wet conditions predominated before cal BP 8700, which brought the expansion of swamp forests areas along the coast (Maldonado and Rozas, 2008; Maldonado and Villagrán, 2006). This wet period was followed by a long-lasting arid phase between cal BP 8700 and 5700. Regional aridity matches the relative dry conditions detected in the first portion of our pollen reconstruction from core BGGC5 in the Guanaqueros Bay, which is represented by relative low values of the Pollen Moisture Index in Fig. 9. Similarly, a general increase in regional precipitation after cal BP ~6000 , observed in pollen records from the northern margin of SWW (Jenny et al., 2003; Maldonado and Villagrán, 2006) is broadly correlated with the observed long-term trend towards increased precipitation observed in the Pollen Moisture after cal BP ~6850. This is also in agreement with Al and Pb, usually considered to be indicators of continental particles that enter to marine waters by fluvial or aerial transport (Calvert and Pedersen, 2007; Govin et al., 2012; Ohnemus and Lam, 2015; Saito et al., 1992; Xu et al., 2015). In our cores, these elements showed trend similar to the pollen record, i.e., a gradual rise in time, suggesting increased humid conditions during recent periods (Fig.9).

In addition, our records indicate long-term increases in grain size and K/Ca ratios and Fe over the last ~8000 years. These increases point to a higher continental inputs most probably caused by increasing rainfall events, which are an important source of sands and K in the northern Chilean margin at the present. Increments of Fe have been documented to provide a boost in primary productivity analyzed in sedimentary records (Dezileau et al., 2004). In our cores, a short-term increase in Fe concentrations is observed between cal BP ~4100 −3600 at the Guanaqueros core, whereas persistent high values are recorded in the Tongoy core between cal BP 7800 − 6500. These two increases coincide with periods with relatively high primary productivity based on the diatoms and opal distribution. This correlation supports the role of Fe as promoter of coastal productivity in the past. However, we note that maximum productivity observed at cal BP ~6700 seems at odd with the overall dry environmental conditions evidence by the pollen data. An explanation for this discrepancy is that dry conditions were more likely associated with increases in SPSH activity in the region and consequently with higher upwelling (Frugone- Álvarez et al., 2017). The subsequent weakening in paleoproductivity after cal BP 6000 can be explained by a reduction in upwelling due to reduced SPSH activity and by the intrusion of less nutrient-enriched upwelled waters over the shelf, influenced by remote equatorial waves, as it is observed today.

The synchronism between highest productivity and dry conditions prior to ~cal BP 6700 highlights the role of the SPSA as an important driver of paleoproductivity changes in the coast of semi-arid Chile during the early portion of the Holocene Period. On the other hand, the pollen and trace element record show both a coherent pattern of increasing humidity and continental discharge over the last 7000 years. The driver of this long-term paleoclimate trend seems to be associated with past shifts in the position of the SWW. In particular, an equatorial displacement of the SWW during mid and later part of the Holocene period, has been suggested by reconstructions from terrestrial and marine proxies (Veit, 1996; Lamy et al., 1999; Lamy et al. 2010).

Studies of coastal upwelling from the Central Peruvian and south Central Chilean coasts (12 − 36 °S) show that present-day wet/dry variability associated with El Niño Southern Oscillation exert an important influence on the bottom ocean oxygenation (Escribano et al., 2004; Gutiérrez et al., 2008; Sellanes et al., 2007). In this regard, OMZs is expected to be less intense during warm El Niño phases and vice versa. This link has been observed by recent studies, as warm events in the Tropical Pacific tend to be associated with low productivity and weak OMZ in the Peruvian coast (Salvatteci et al., 2014). An increase in the frequency of ENSO-like warm events could, therefore, explain the reduction in productivity recorded after cal BP 6700 in our records. In this case, warm events in the eastern Pacific could have reduced the ocean productivity and organic fluxes from primary productivity and overall dropping oxygen consumption during organic matter diagenesis. In the light of these mechanisms, our results suggest more El Niño-like conditions during the latter part of the Holocene, an inference that is consistent with the available evidence for an increase in the frequency of El Niño events over the last 4000–5000 years (Conroy et al., 2008; Moy et al., 2002). We further note that present-day El Niño years are generally connected with increased westerly flow over central Chile including the semi-arid region (Montecinos and Aceituno, 2003), and therefore more frequent El Niño states during the latter part of the Holocene are also consistent with a long-term increase in precipitation revealed by the pollen and trace element data.

6. Conclusions

Our result indicates that the ocean circulation at our study sites seems to affect both places differently, leaving more variable grain compositions and higher TOC contents in the Guanaqueros Bay (core BGGC5) than in the Tongoy Bay (core BTGC8). This difference should be interpreted as an increase in the time of particle transportation resulting in grain size selection (more leptokurtic at core BTGC8), especially after cal BP 2000. Furthermore, in both bays, constantly decreasing TOC contents were observed after cal BP ~4000 to the present, probably due to higher oxygenation of the bay bottom in time.

Differences in redox conditions in our records could be reconstructed in detail, showing a clear decreasing trend in oxygen bottoms before the beginning of recent time (cal BP ~2000), followed by a rapid change to a more oxygenated environment. The environmental conditions at bottom waters was essential in the metal enrichment factor above crustal abundance within the sediments (highest EFs), since low organic carbon accumulation and low sedimentation rates have been estimated, indicating that the accumulation of these elements (U, Mo and Re) depends mainly on oxygen content instead of on organic carbon burial rates. Our result suggest that a maximum suboxia-anoxia occurred at cal BP ~6700, when peak U and Re where recorded, probably due to the presence of a sulfidic environment.

The nutrient-type elements follow a similar trend, reduced at present and showing higher accumulation rates around cal BP 6700 (Ca, Ni, P and Cd). Their distribution is consistent with the diatom and opal distributions, showing their dependence on primary productivity and organic carbon burial rates. If the kinetics reaction is working at low rates for these elements, they should be highly influenced during oxygenation periods, something that seems to have been operating at higher frequencies.

The record of continental proxies suggests a long-term increase in precipitation, consistent with previous reconstructions in central Chile. The most distinctive changes were observed after cal BP 6500 – 6700 when an overall expansion of the coastal vegetation occurred as a result of a progressive increase in precipitation and river runoffs, expanding the grain size of the sediments and the higher concentrations of elements with an important continental source (Al, Fe, K and Pb).
Increased regional precipitations amounts have been commonly interpreted by a northward shift of the Southern Westerly Winds belts, yet the increased frequency of El Niño events did more likely introduce a high variability of humidity after cal BP 5000. Thus, the apparent increase of oxygen conditions at bottoms could have been the result of this oceanographic feature, which introduced a more oxygenated water mass to the shelf and bays, temporarily changing the redox conditions in surface sediments and affecting the sensitive elements to redox potential change in the environment. Additionally, this also affected the accumulation of organic matter due to an intensification of its remineralization, showing a decreasing trend in nutrient type element accumulation and organic carbon burial rates towards the present.
Finally, our results suggest that the geochemistry and sedimentary properties of coastal shelf environments in North-central Chile have changed considerably during the Holocene period. In particular, decreasing trends in primary productivity highlight the sensitivity of these environments to regional climate changes at different timescales. Future changes are therefore likely to be expected in the ongoing scenario of environmental changes at unprecedented rates.

7. References

Abrantes, F.: Diatom assemblages as upwelling indicators in surface sediments off Portugal, Mar. Geol., 85(1), 15–39, doi:10.1016/0025-3227(88)90082-5, 1988.

Ancapichún, S., Garcés-Vargas, J.: Variability of the Southeast Pacific Subtropical Anticyclone and its impact on sea surface temperature off north-central Chile Variabilidad del Anticiclón Subtropical del Pacífico Sudeste y su impacto sobre la temperatura superficial del mar frente a la costa centro-norte de Chile, Cienc. Mar., 41(1), 1–20, http://dx.doi.org/10.7773/cm.v41i1.2338, 2015.

Appleby, P. G. and Oldfield, F.: The calculation of lead-210 dates assuming a constant rate of supply of unsupported210Pb to the sediment, Catena, 5(1), 1–8, doi:10.1016/S0341-8162(78)80002-2, 1978.

Behrenfeld, M. J., O'Malley, R. T., Siegel, D. A., McClain, C. R., Sarmiento, J. L., Feldman, G. C., Milligan, A. J., Falkowski, P. G., Letelier, R. M. and Boss, E. S.: Climate-driven trends in contemporary ocean productivity, Nature, 444(7120), 752–755, doi:10.1038/nature05317, 2006.

Bevington, P. and Robinson, K. (Eds.): Error analysis. In: Data Reduction and Error Analysis for the Physical Sciences, WCB/McGraw-Hill, USA, 38–52, 1992

Blasco, D., Estrada, M. and Jones, B. H.: Short time variability of phytoplankton populations in upwelling regions-the example of Northwest Africa. In: Coastal upwelling. F. A. Richards (Ed.), AGU Washington DC, 339 – 347, 1981

Blott, S. J. and Pye, K.: Gradistat: A Grain Size Distribution and Statistics Package for the Analysis of Unconcolidated Sediments, Earth Surf. Process. Landforms, 26, 1237–1248, doi:10.1002/esp.261, 2001.

Bolin, B.: The carbon cycle and global change: a focus on CO2. In: Trace Gases and the Biosphere. Moore, B. III and Schimel, D. (Eds.), Boulder: University Corporation for Atmospheric Research, 129−149, 1992.

Calvert, S. E. and Pedersen, T. F.: Geochemistry of Recent oxic and anoxic marine sediments: Implications for the geological record, Mar. Geol., 113(1–2), 67–88, doi:10.1016/0025-3227(93)90150-T, 1993.

Calvert, S. E. and Pedersen, T. F.: Chapter Fourteen Elemental Proxies for Palaeoclimatic and Palaeoceanographic Variability in Marine Sediments: Interpretation and Application, Dev. Mar. Geol., 1(7), 567–644, doi:10.1016/S1572-5480(07)01019-6, 2007.

Carré, M., Jackson, D., Maldonado, A., Chase, B.M., Sachs, J.P.: Variability of 14C reservoir age and air–sea flux of CO2 in the Peru–Chile upwelling region during the past 12,000 years, Quat. Res., 85, 87–93, 2016.

Merino-Campos, V., De Pol-Holz, R. Southon, J., Latorre, C., Collado-Fabbri, S.: Marine radiocarbon reservoir age along the Chilean continental margin, Radiocarbon, 81, 1–16, doi:10.1017/RDC.2018.81, 2018.

Cha, H. J., Lee, C. B., Kim, B. S., Choi, M. S. and Ruttenberg, K. C.: Early diagenetic redistribution and burial of phosphorus in the sediments of the southwestern East Sea (Japan Sea), Mar. Geol., 216(3), 127–143, doi:10.1016/j.margeo.2005.02.001, 2005.

Chaillou, G., Anschutz, P., Lavaux, G., Schäfer, J. and Blanc, G.: The distribution of Mo, U, and Cd in relation to major redox species in muddy sediments of the Bay of Biscay, Mar. Chem., 80(1), 41–59, doi:10.1016/S0304-4203(02)00097-X, 2002.

Chester, R.: Redox environments and diagenesis in marine sediments, In: Marine Geochemistry, Chapman & Hall, 486–524, 1990.

Colodner, D., Sachs, J., Ravizza, G., Turekian, K. K. and Boyle, E.: The geochemical cycle of Re: a reconnaissance, Earth Planet. Sci. Lett., 117, 205–221, doi:10.1016/0012-821X(93)90127-U, 1993.

Conroy, J.L., Overpeck, J.T., Cole, J.E., Shanahan, T.M., Steinitz-Kannan, M.: Holocene changes in eastern tropical Pacific climate inferred from a Galápagos lake sediment record. Quat. Sci. Rev., 27, 1166-1180, 2008.

Crusius, J., Calvert, S., Pedersen, T. and Sage, D.: Rhenium and molybdenum enrichments in sediments as indicators of oxic, suboxic and sulfidic conditions of deposition, Earth Planet. Sci. Lett., 145(1–4), 65–78, doi:10.1016/S0012-821X(96)00204-X, 1996.

Cupp, E.E.: Marine plankton diatoms of the west coast of North America, Bulletin of the Scripps Institution of Oceanography 5, 1–238, 1943.

Daneri, G., Dellarossa, V., Quiñones, R., Jacob, B., Montero, P. and Ulloa, O.: Primary production and community respiration in the Humboldt Current System off Chile and associated oceanic areas, Mar. Ecol. Prog. Ser., 197, 41–49, doi:10.3354/meps197041, 2000.

Dearing, J., Magnetic susceptibility. In: Environmental Magnetism: A Practical Guide. Walden, J., Oldfield, F., and Smith, J. (Eds.), Quaternary Research Association Technical Guide No. 6, London, 35–62, 1999.

De Pol-Holz, R., Ulloa, O., Lamy, F., Dezileau, L., Sabatier, P., and Hebbeln, D.: Late Quaternary variability of sedimentary nitrogen isotopes in the eastern South Pacific Ocean, Paleoceanography, 22, PA2207, doi: 10.1029/2006 PA001308, 2007.

Dezileau, L., Ulloa, O., Hebbeln, D., Lamy, F., Reyss, J. L. and Fontugne, M.: Iron control of past productivity in the coastal upwelling system off the Atacama Desert, Chile, Paleoceanography, 19(3), doi:10.1029/2004PA001006, 2004.

Dymond, J., Suess, E. and Lyle, M.: Barium in deep-sea sediment: A geochemical proxy for paleoproductivity, Paleoceanography, 7(2), 163‒181, 1992.

Escribano, R., Daneri, G., Farías, L., Gallardo, V. A., González, H. E., Gutiérrez, D., Lange, C. B., Morales, C. E., Pizarro, O., Ulloa, O. and Braun, M.: Biological and chemical consequences of the 1997-1998 El Niño in the Chilean coastal upwelling system: A synthesis, Deep. Res. Part II Top. Stud. Oceanogr., 51(20–21), 2389–2411, doi:10.1016/j.dsr2.2004.08.011, 2004.

Faegri, K. and Iversen, J.: Textbook of pollen analysis, IV. The Blackburn Press, New Yersey, 328 pp., 1989.

Filippelli, G. M.: Controls on phosphorus concentration and accumulation in oceanic sediments, Mar. Geol., 139, 231-240, 1997.

Flynn, W. W.: The determination of low levels of polonium-210 in environmental materials, Anal. Chim. Acta, 43, 221–227, 1968.

Frugone-Álvarez, M., Latorre, C., Giralt, S., Polanco-Martínez, J., Bernárdez, P., Oliva-Urcia, B., Maldonado, A., Carrevedo, M. L., Moreno, A., Delgado Huertas, A., Prego, R., Barreiro-Lostres, F. and Valero-Garcés, B.: A 7000-year high-resolution lake sediment record from coastal central Chile (Lago Vichuquén, 34°S): implications for past sea level and environmental variability, J. Quat. Sci., 32(6), 830–844, doi:10.1002/jqs.2936, 2017.

Gallardo, M.A., González, A., Ramos, M., Mujica, A., Muñoz, P., Sellanes, J., Yannicelli, B.: Reproductive patterns in demersal crustaceans from the upper boundary of the OMZ off north-central Chile, Cont. Shelf. Res. 141, 26–37, 2017. http://dx.doi.org/10.1016/j.csr.2017.04.011

Ganeshram, R.S., Pedersen, T. F., Calvert, S.G.,McNeill, G., Fontugne, M.: Glacial-interglacial variability in denitrification in the world's oceans: Causes and consequences. Paleoceanography, 15(4), 361– 376, 2000.

Garreaud, R. and Rutllant, J.: Análisis meteorológico de los aluviones de Antofagasta y Santiago de Chile en el período 1991–1993, Atmósfera, 9, 251–271, 1996.

Garreaud, R., Vuille. M., Compagnuccic, R. and Marengo, J.: Present-day South American climate, Palaeogeogr. Palaeocl., 281, 180-195, doi:10.1016/j.palaeo.2007.10.032

González, H. E., Daneri, G., Figueroa, D., Iriarte, J., Lefèvre, N., Pizarro, G., Quiñones, R., Sobarzo, M. and Troncoso, A.: Producción primaria y su destino en la trama trófica pelágica y océano profundo e intercambio océano-atmósfera de CO2 en la zona norte de la Corriente de Humboldt (23º S): posibles efectos del evento El Niño 1997. Rev. Chil. Hist. Nat., 71, 429-458, 1998.

Govin, A., Holzwarth, U., Heslop, D., Ford Keeling, L., Zabel, M., Mulitza, S., Collins, J. A. and Chiessi, C. M.: Distribution of major elements in Atlantic surface sediments

(36°N-49°S): Imprint of terrigenous input and continental weathering, Geochemistry, Geophys. Geosystems, 13(1), 1–23, doi:10.1029/2011GC003785, 2012.

Guieu, C., Martin, J. M., Tankéré, S. P. C., Mousty, F., Trincherini, P., Bazot, M., Dai, M. H.: On trace metal geochemistry in the western Black Sea: Danube and shelf area. Estuarine, Coastal and Shelf Science, 47, 471–485, 1998.

Gitiérrez, D., Sifedine, A., Reyss, J.L., Vargas, G., Velazco, F., Salvattci, R., Ferreira, V., Ortlieb, L., Field, D., Baumgartner, T., Boussafir, M., Boucher, H., Valdés, J., Marinovic, L., Soler, P., Tapia, P: Anoxic sediments off Central Peru record interannual to multidecadal changes of climate and upwelling ecosystem during the last two centuries, Adv. Geosci. 6, 119–125, 2006.

Gutiérrez, D., Enríquez, E., Purca, S., Quipuzcoa, L., Marquina, R., Flores, G. and Graco, M.: Oxygenation episodes on the continental shelf of central Peru: Remote forcing and benthic ecosystem response. Prog. Oceanogr., 79, 177–189, 2008.

Gutiérrez, D., Sifeddine, A., Field, D. B.,, Ortlieb, L-., Vargas, G., Chávez, F.P., Velazco, F., Ferreira, V., Tapia, P., Salvatteci, R., Boucher, H., Morales, M.C., Valdés, J., Reyss, J.-L., Campusano, A., Boussafir, M., Mandeng-Yogo, M., García, M., Baumgartner, T.:Rapid reorganization in ocean biogeochemistry off Peru towards the end of the Little Ice Age, Biogeosciences, 6, 835–848, 2009.

Hansen, H. P., Koroleff, F.: Determination of nutrients. In Methods of Seawater Analysis. Grasshoff, K., Kremling, K. and Ehrhardt, M. (Eds.), Wiley-VCH Verlag GmbH, Weinheim, Germany, 159–228, 1999.

Hatfield, R. G., Stoner, J. S.: Magnetic Proxies and Susceptibility. In: The Encyclopedia of Quaternary Science. Elias, S.A. (ed.) 2, 884-898, 2013.

Hebbeln, D., Marchant, M., Freudenthal, T., Wefer, G.: Surface distribution along the Chilean continental slope related to upwelling and productivity. Marine Geology 164, 119–137, 2000.

Hebbeln, D., Marchant, M. and Wefer, G.: Paleoproductivity in the southern Peru ^ Chile Current through the last 33 000 yr, Mar. Geol., 186, 2002.

Helly, J. and Levin. L.: Global distribution of naturally occurring marine hypoxia on continental margin, Deep-Sea Res. Pt. I, 51, 1159-1168, 2004.

Heusser, C. J. and Moar, N. T.: Pollen and spores of chile: Modern types of the pteridophyta, gymnospermae, and angiospermae, New Zeal. J. Bot., 11(2), 389–391, doi:10.1080/0028825X.1973.10430287, 1973.

Higginson, M.J:, Altabet, M.A., Wincze, L., Herbert, D., Murray, D.: A solar (irradiance) trigger for millennial-scale abrupt changes in the southwest monsoon? Paleoceanography, 19, PA3015, doi:10.1029/2004PA001031, 2004.

Huerta-Diaz, M. A. and Morse, J. W.: Pyritization of trace metals in anoxic marine sediments, Geochim. Cosmochim. Acta, 56(7), 2681–2702, doi:10.1016/0016-7037(92)90353-K, 1992.

Jöris, O. and Weninger, B.: Extension of the C-14 calibration curve to ca. 40,000 cal BC by synchronizing Greenland O-18/O-16 ice core records and North Atlantic foraminifera profiles: A comparison with U/Th coral data, Radiocarbon, 40(1), 495–504, doi:10.2458/azu_js_rc.40.2036, 1998.

Kaiser, J., Schefuß, E., Lamy, F., Mohtadi, M., Hebbeln, D.:Glacial to Holocene changes in sea surface temperature and coastal vegetation in north central Chile: high versus low latitude forcing, Quat. Sci. Rev., 27, 2064–2075, 2008.

Keshav, N. and Achyuthan, H.: Late Holocene continental shelf sediments, off Cuddalore, East coast, Bay of Bengal, India: Geochemical implications for source-area weathering and provenance, Quat. Int., 371, 209–218, doi:10.1016/j.quaint.2015.03.002, 2015.

Klinkhammer, G. P. and Palmer, M. R. Uranium in the oceans: Where it goes and why, Geochim. Cosmochim. Ac., 55(7), 1799–1806, doi: 10.1016/0016-037(91)90024-Y, 1991.

Koutavas, A., deMenocal, P.B., Olive, G.C., Lynch-Stieglitz, J.: Mid-Holocene El Nin˜o–Southern Oscillation (ENSO) attenuation revealed by individual foraminifera in eastern tropical Pacific sediments, 34(12), 993–996, doi: 10.1130/G22810A, 2006.

Lamy F., Hebbeln, D., Wefer, G.: High-Resolution Marine Record of Climatic Change in Mid-latitude Chile during the Last 28,000 Years Based on Terrigenous Sediment Parameters, Quat. Res., 51**,** 83–93, 1999.

Lamy, F., Hebbeln, D., Röhl, U. and Wefer, G.: Holocene rainfall variability in southern Chile: a marine record of latitudinal shifts of the Southern Westerlies. Earth Planet. Sc. Lett., 185, 369–382, 2001.

Lamy, F., Rühlemann, C., Hebbeln, D. and Wefer, G.: High- and low-latitude climate control on the position of the southern Peru-Chile Current during the Holocene, Paleoceanography, 17(2), 16-1-16–10, doi:10.1029/2001PA000727, 2002.

Lamy, F., Kilian, R., Arz, H.W., Francois J-P., Kaiser, J.,Prange, M. and Steinke, T.: Holocene changes in the position and intensity of the southern westerly wind belt, Nat. Geosci., 3, 695–699, 2010.

Little, S. H., Vance, D., Walker-Brown, C. and Landing, W. M.: The oceanic mass balance of copper and zinc isotopes, investigated by analysis of their inputs, and outputs to ferromanganese oxide sediments, Geochim. Cosmochim. Acta, 125, 673–693, doi:10.1016/j.gca.2013.07.046, 2014.

Maldonado, A. and Rozas, E.: Clima y Paleoambientes durante el Cuaternario Tardío en la Región de Atacama, in Libro Rojo de la Flora Nativa y de los Sitios Prioritarios para su Conservación: Región de Atacama, pp. 293–304., 2008.

Maldonado, A. and Villagrán, C.: Climate variability over the last 9900 cal yr BP from a swamp forest pollen record along the semiarid coast of Chile, Quat. Res., 66(2), 246–258, doi:10.1016/j.yqres.2006.04.003, 2006.

Marchant, M., Hebbeln, D. and Wefer, G.: High resolution foraminiferal record of the last 13,300 yeras from the upwelling area off Chile, Mar. Geol., 161, 115–128, doi:https://doi.org/10.1016/S0025-3227(99)00041-9, 1999.

Marín, V. H., Delgado, L. E. and Luna-Jorquera, G.: S-chlorophyll squirts at 30°S off the Chilean coast (eastern South Pacific): Feature-tracking analysis. J. Geophys. Res., 108(12), 3378 – 3384, doi:10.1029/2003JC001935, 2003.

Mazzullo, J., Gilbert, A., Rabinowitz, P., Meyer, A. and Garrison, L.: Handbook for Shipboard Sedimentologists, 67 pp., 1988.

McManus, J., Nägler, T. F., Siebert, C., Wheat, C. G. and Hammond, D. E.: Oceanic molybdenum isotope fractionation: Diagenesis and hydrothermal ridge-flank alteration. Geochem. Geophy. Geosy., 3(12), 1–9, 2002.

Mohtadi, M., Rossel, P., Lange, C.B., Pantoja, S., Böning, P., Repeta, D., Grunwald, M., Lamy, F., Hebbeln, D., Brumsack, H-J.: Deglacial pattern of circulation and marine productivity in the upwelling region off central-south Chile, Earth Planet. Sci. Lett. , 272, 221–230, 2008.

Montecinos, A., and Aceituno, P.: Seasonality of the ENSO-Related Rainfall Variability in Central Chile and Associated Circulation Anomalies. J. Climate., 16, 281–296. https://doi.org/10.1175/1520-0442(2003)016<0281:SOTERR>2.0.CO;2, 2003.

Montecinos, S., Gutiérrez, J. R., López-Cortés, F. and López, D.: Climatic characteristics of the semi-arid Coquimbo Region in Chile, J. Arid Environ., 126, 7–11, doi:10.1016/j.jaridenv.2015.09.018, 2015.

Moraga-Opazo, J., Valle-Levinson, A., Ramos, M. and Pizarro-Koch, M.: Upwelling-Triggered near-geostrophic recirculation in an equatorward facing embayment, Cont. Shelf Res., 31, 1991–1999, 2011.

Mortlock, R. A. and Froelich, P. N.: A simple method for the rapid determination of biogenic opal in pelagic marine sediments, Deep Sea Res. Part A, Oceanogr. Res. Pap., 36(9), 1415–1426, doi:10.1016/0198-0149(89)90092-7, 1989.

Mosley-Thompson, E., Thompson, L. G. and Lin, P. N.: A multi-century ice-core perspective on 20th-century climate change with new contributions from high-Arctic and Greenland (PARCA) cores, Ann. Glaciol., 43, 42–48, doi:10.3189/172756406781812401, 2006.

Morse, J.W. and Luther, G.W.: Chemical influences on trace metal–sulfide interactions in anoxic sediments. Geochim Cosmochim Ac., 63, 3373–3378, 1999.

Moy, C.M., Seltzer, G.O., Rodbell, D.T. and Anderson, D.M.: Variability of El Niño/Southern Oscillation activity at millennial timescales during the Holocene epoch. Nature, 420(6912), p.162, 2002.

Muñoz, P., Dezileau, L., Dezileau, L., Lange, C.B., Cardenas, L., Sellanes, J., Salamanca, M.A., Maldonado, A.: Evaluation of sediment trace metal records as paleoproductivity and paleoxygenation proxies in the upwelling center off Concepción, Chile (36°S)., Prog. Oceanogr., 92–95, 66–80, 2012.

Nakanishi, T. and Minagawa, M.: Stable carbon and nitrogen isotopic compositions of sinking particles in the northeast Japan Sea, Geochem. J., 37(2), 261–275, doi:https://doi.org/10.2343/geochemj.37.261, 2003.

Nameroff, T., Balistrieri, L. and Murray, W.: Suboxic trace metals geochemistry in the eastern tropical North Pacific, Geochim Cosmochim Ac., 66(7), 1139–1158, 2002.

Nurhati, I. S., Cobb, K. M., Charles, C. D. and Dunbar, R. B.: Late 20th century warming and freshening in the central tropical Pacific, Geophys. Res. Lett., 36(21), 2–5, doi:10.1029/2009GL040270, 2009.

Ogrinc, N., Fontolan, G., Faganeli, J. and Covelli, S.: Carbon and nitrogen isotope compositions of organic matter in coastal marine sediments (the Gulf of Trieste, N Adriatic Sea): indicators of sources and preservation, Mar. Chem., 95, 163-181, 2005.

Ohnemus, D. C. and Lam, P. J.: Cycling of lithogenic marine particles in the US GEOTRACES North Atlantic transect, Deep. Res. Part II Top. Stud. Oceanogr., 116, 283–302, doi:10.1016/j.dsr2.2014.11.019, 2015.

Paytan, A.: Ocean paleoproductivity, Encyclopedia of Paleoclimatology and Ancient Environments, Encyclopedia of Earth Science Series, Gornitz, V. (Ed.), Kluwer Academic Publishers. 2008.

Peacock, C.L. and Sherman, D.M.: Copper(II) sorption onto goethite, hematite and lepidocrocite: a surface complexation model based on ab initio molecular geometries and EXAFS spectroscopy. Geochim. Cosmochim. Ac., 68, 2623–2637, 2004.

Pizarro, O., Shaffer, G., Dewitte, B. and Ramos, M.: Dynamics of seasonal and interannual variability of the Peru-Chile Undercurrent, Geophys. Res. Lett., 29(12), 28–31, doi:10.1029/2002GL014790, 2002.

Ramos, M., Pizarro,O., Bravo, L. and Dewitte, B.: Seasonal variability of the permanent thermocline off northern Chile, Geophys. Res. Lett., 33, L09608, doi:10.1029/2006GL025882, 2006.

Ramos, M., Dewitte, B., Pizarro, O. and Garric, G.: Vertical propagation of extratropical Rossby waves during the 1997–1998 El Niño off the west coast of South America in a medium-resolution OGCM simulation, J. Geophys. Res., 113, C08041, doi:10.1029/2007JC004681, 2008.

Rau, H. G., Takahashi, T. and Des Marais, D. J.: Latitudinal variations in plankton δ13C: implications for CO2 and productivity in past oceans, Nature, 341, 516–518, 1989.

Reimer, P. J., Bard, E., Bayliss, A., Beck, J. W., Blackwell, P. G., Ramsey, C. B., Buck, C. E., Cheng, H., Edwards, R. L., Friedrich, M., Grootes, P. M., Guilderson, T. P., Haflidason, H., Hajdas, I., Hatté, C., Heaton, T. J., Hoffmann, D. L., Hogg, A. G., Hughen, K. A., Kaiser, K. F., Kromer, B., Manning, S. W., Niu, M., Reimer, R. W., Richards, D. A., Scott, E. M., Southon, J. R., Staff, R. A., Turney, C. S. M. and van der Plicht, J.: IntCal13 and Marine13 Radiocarbon Age Calibration Curves 0–50,000 Years cal BP, Radiocarbon, 55(4), 1869–1887, doi:10.2458/azu_js_rc.55.16947, 2013.

Rein, B., Lückge, A., Sirocko, F.,: A major Holocene ENSO anomaly during Medieval period, Geophys. Res. Lett. 31, L17211, doi:10.1029/2004GL020, 2004

Rivera, P.: Beiträge zur Taxonomie und Verbreitung der Gattung Thalassiosira Cleve. Bibl. Phycol., 56, 1–220, 1981.

Rodbell, D.T., Seltzer, G.O., Anderson, D.M., Abbott, M.B, Enfield, D.B, Newman JH: An approximately 15,000-year record of El Nino-driven alluviation in southwestern Ecuador, Science, 283, 516 – 520, 1999.

Round, E. E., Crawford, R. M. and Mann, D.G.: The Diatoms: biology and morphology of the genera. Cambridge University Press, Cambridge, 747 pp., 1990.

Romero, O., Kim, J-H, Hebbeln, D.: Paleoproductivity evolution off central Chile from the Last Glacial Maximum to the Early Holocene, Quat. Res., 65, 519 – 525, 2006.

Saavedra ‐ Pellitero,M., Flores, J. A., Lamy, F., Sierro, F. J., Cortina, A.: Coccolithophore estimates of paleotemperature and paleoproductivity changes in the southeast Pacific over the past ∼27 kyr.

Sabatier, P., Dezileau, L., Blanchemanche, P., Siani, G., Condomines, M., Bentaleb, I. and Piquès, G.: Holocene variations of radiocarbon reservoir ages in a mediterranean lagoonal system, Radiocarbon, 52(1), 91–102, doi:10.1017/S0033822200045057, 2010.

Saito, C., Noriki, S. and Tsunogai, S.: Particulate flux of Ai, a component of land origin, in the western North Pacific, Deep-Sea Res., 39, 1315–1327, 1992.

Salvatteci, R., Gutiérrez, D., Field, D., Sifeddine, A., Ortlieb, L., Bouloubassi, I., Boussafir, M., Boucher, H. and Cetin, F.: The response of the Peruvian Upwelling Ecosystem to centennial-scale global change during the last two millennia, Clim. Past, 10(2), 715–731, doi:10.5194/cp-10-715-2014, 2014.

Sarmiento, J. L. and Gruber, N.: Sinks for Anthropogenic Carbon, Phys. Today, 55(8), 30–36, doi:10.1063/1.1510279, 2002.

Schneider, D. P. and Steig, E. J.: Ice cores record significant 1940s Antarctic warmth related to tropical climate variability, Proc. Natl. Acad. Sci., 105(34), 12154–12158, doi:10.1073/pnas.0803627105, 2008.

Schrader H. J. and Gersonde, R.: Diatoms and silicoflagellates. Utrecht Micropaleontol. Bull. 17, 129–176, 1978.

Sellanes, J. , Quiroga, E., Neira, C., Gutiérrez, D., : Changes of macrobenthos composition under different ENSO cycle conditions on the continental shelf off central Chile, Cont. Shelf. Res. 27, 1002 –1016, 2007.

Shaffer, G., Pizarro, O. Djurfeldt, L., Salinas, S. and Rutllant, J.: Circulation and low-frequency variability near the Chilean coast: Remotely forced fluctuations during the 1991– 92 El Niño, J. Phys. Oceanogr., 27, 217– 235, 1997.

Siebert, C., Nägler, T. F., von Blanckenburg, F., and Kramers, J. D.: Molybdenum isotope records as a potential new proxy for paleoceanography, Earth Planet. Sc. Lett., 211(1), 159–171, 2003.

Sigman, D.M., Karsh, K.L., Casciotti, K.L.: Ocean process tracers: nitrogen isotopes in the ocean. Encyclopedia of ocean science, 2nd edn Elsevier, Amsterdam.

Sims, P.A. 1996. An Atlas of British Diatoms. Biopress Ltd, Bristol United Kingdom 601, 2009.

Sun, X., Higgins, J. and Turchyn, A. V.: Diffusive cation fluxes in deep-sea sediments and insight into the global geochemical cycles of calcium, magnesium, sodium and potassium, Mar. Geol., 373, 64–77, doi:10.1016/j.margeo.2015.12.011, 2016.

Sundby, B., Martinez, P. and Gobeil, C.: Comparative geochemistry of cadmium, rhenium, uranium, and molybdenum in continental margin sediments, Geochim. Cosmochim. Ac., 68, 2485–2493, 2004.

Sweeney, R. E., Kaplan I. R.: Natural abundances of 15N as a source indicator of nearshore marine sedimentary and dissolved nitrogen, Mar. Chem., 9, 81‒94, 1980.

Thomas, C. D., Bodsworth, E. J., Wilson, R. J., Simmons, A. D., Davies, Z. G., Musche, M. and Conradt, L.: Ecological and evolutionary processes at expanding range margins, Nature, 411, 577‒581, 2001.

Torres, M. E., Brumsack, H. J., Bohrman, G. and Emeis, K. C.: Barite front in continental margin sediments: a new look at barium remobilization in the zone of sulfate reduction and formation of heavy barites in diagenetic fronts, Chem. Geol., 127, 125–139, 1996.

Torres, R., and Ampuero, P.: Strong CO2 outgassing from high nutrient low chlorophyll coastal waters off central Chile (30°S): The role of dissolved iron, Estuar. Coast. Shelf S., 83, 126‒132, doi:10.1016/j.ecss.2009.02.030, 2009.

Tribovillard, N., Algeo, T. J., Lyons, T. and Riboulleau, A.: Trace metals as paleoredox and paleoproductivity proxies: an update. Chem. Geol., 232, 12–32, 2006.

Vance, D., Archer, C., Bermin, J., Perkins, J., Statham, P. J., Lohan, M. C., Ellwood, M. J. and Mills, R. A.: The copper isotope geochemistry of rivers and the oceans, Earth Planet. Sc. Lett., 274, 204–213, 2008.

Valle-Levinson, A., Moraga, J., Olivares, J. and Blanco, J. L.: Tidal and residual circulation in a semi-arid bay: Coquimbo Bay, Chile. Cont. Shelf Res., 20, 2009–2018, 2000.

Valle-Levinson, A. and Moraga-Opazo, J.: Observations of bipolar residual circulation in two equatorward-facing semiarid bays, Cont. Shelf Res., 26(2), 179–193, doi:10.1016/j.csr.2005.10.002, 2006.

Van der Weijden, C.: Pitfalls of normalization of marine geochemical data using a common divisor, Mar. Geol., 184, 167–187, 2002.

Vargas, G., Ortlieb, L., Pichon, J. J., Bertaux, J. and Pujos, M.: Sedimentary facies and high resolution primary production inferences from laminated diatomacous sediments off northern Chile (23°S), Mar. Geol., 211(1–2), 79–99, doi:10.1016/j.margeo.2004.05.032, 2004.

Vargas, G., Rutllant, J., Ortlieb, L.: ENSO tropical–extratropical climate teleconnections and mechanisms for Holocene debris flows along the hyperarid coast of western South America (17°–24°S), Earth Planet. Sci. Lett., 249, 467–483, 2006.

Vargas, G., Pantoja, S., Rutllant, J., Lange, C. and Ortlieb, L.: Enhancement of coastal upwelling and interdecadal ENSO-like variability in the Peru-Chile Current since late 19th century. Geophys. Res. Lett., 34, L13607, 2007.

Varma, V., Prange, M., Merkel, U., Kleinen, T., Lohmann, G., Pfeiffer, M., Renssen, H., Wagner, A. and Schulz, M.: Holocene evolution of the Southern Hemisphere westerly winds in transient simulations with global climate models. Clim. Past, 8, 391–402, doi:10.5194/cp-8-391-2012, 2012.

Veit, H.: Southern Westerlies during the Holocene deduced from geomorphological and pedological studies in the Norte Chico, Northern Chile (27–33°S). *Palaeogeogr., Palaeoclimatol., Palaeoecol.,* 123**,** 107–119, 1996.

Wells, D. V., Hill, J. M., Park, M. J. and Williams, C. P.: The Shallow Sediments of the Middle Chincoteague Bay Area in Maryland: Physical and Chemical Characteristics. (Coastal and Estuarine Geology File Report No. 98-1): Maryland Geological Survey, Baltimore, MD., 104 pp., 1998.

Williams, P. M. and Gordon, L. I.: Carbon-13:carbon-12 ratios in dissolved and particulate organic matter in the sea. Deep-Sea Res., 17, 19–27, 1970.

Xu, G., Liu, J., Pei, S., Kong, X., Hu, G. and Gao, M.: Source identification of aluminum in surface sediments of the Yellow Sea off the Shandong Peninsula, Acta Oceanol. Sin., 34(12), 147–153, doi:10.1007/s13131-015-0766-9, 2015.

Zheng, Y., van Geen, A., Anderson, R. F., Gardner, J. V. and Dean, W. E.: Intensification of the northeast Pacific oxygen minimum zone during the Bölling-Alleröd warm period, Paleoceanography, 15, 528−536, 2000.

Zheng, Y., Anderson, R. F., van Geen, A. and Fleisheir, M.Q.: Preservation of non-lithogenic particulate uranium in marine sediments. Geochim. Cosmochim. Ac., 66, 3085–3092, 2002.

Acknowledgments

We would like to thank the R/V Stella Maris II crew of Universidad Católica del Norte for their help and support during field work. We extend our acknowledgements to the laboratory assistants of the Paleoceanography Lab at Universidad de Concepción, for their aid in sample analyses. We also wish to thank Dr. Olivier Bruguier of CNRS and his lab personnel for their assistance during ICPMs analyses. We also express our gratitude to INNOVA 07CN13 IXM-150. This manuscript was funded by FONDECYT Project No. 1140851. Partial support from the COPAS Sur-Austral (CONICYT PIA PFB31) and FONDAP-IDEAL centers (No. 15150003) is also acknowledged.

Tables

Table 1. Concentration of elements in Pachingo wetland sediments, considered as lithogenic background for the study area. The values correspond to mean concentrations in surface sediments (0−3 cm).

Element	Metal/Al x 10^3	s
Ca	686.5	139.3
Fe	591.3	84.5
P	8.6	0.7
Sr	5.7	0.6
Ba	5.6	0.1
Cu	0.258	0.019
Ni	0.174	0.005
U	0.020	0.003
Mo	0.020	0.003
Cd	0.0021	0.0003
Re	0.00004	0.00001

Table 2. Radiocarbon dates for BGGC5 and BTGC8 sediment cores collected from mixed planktonic foraminifera and monospecific benthic foraminifera (*Bolivina plicata*), respectively. The ^{14}C-AMS was performed at NOSAM-WHOI. The lab code and conventional ages collected from each core section is indicated. For error calculations see http://www.whoi.edu/nosams/radiocarbon-data-calculations.

Core identification	material	mass (mg)	Lab Code NOSAM	Modern fraction pMC	1σ error	Conventional Age BP	1σ error
BGGC5	Planktonic foraminifera						
10-11	mix	1,8	OS-122160	0,8895	0,0027	940	25
18-19	mix	1,1	OS-122141	0,7217	0,0024	2.620	25
31-32	mix	2,7	OS-122161	0,6590	0,0021	3.350	25
45-46	mix	2	OS-122162	0,6102	0,0017	3.970	25
55-56	mix	1,6	OS-122138	0,5864	0,0025	4.290	35
66-67	mix	2,8	OS-122304	0,5597	0,0018	4.660	25
76-77	mix	2,6	OS-122163	0,4520	0,0016	6.380	30
96-97	mix	1,1	OS-122139	0,4333	0,0033	6.720	60
115-116	mix	4,7	OS-122164	0,3843	0,0016	7.680	35
BTGC8	Benthic foraminifera						
5-6	Bolivina plicata	4,2	OS-130657	0,8953	0,0017	890	15
20-21	Bolivina plicata	7,7	OS-123670	0,7337	0,0021	2.490	25
30-31	Bolivina plicata	13	OS-123671	0,6771	0,0016	3.130	20
40-41	Bolivina plicata	11	OS-123672	0,6507	0,0019	3.450	25
50-51	Bolivina plicata	8,7	OS-123673	0,5877	0,0014	4.270	20
60-61	Bolivina plicata	13	OS-123674	0,5560	0,0018	4.720	25
71-72	Bolivina plicata	10	OS-123675	0,4930	0,0013	5.680	20
80-81	Bolivina plicata	7,3	OS-123676	0,4542	0,0012	6.340	20
90-91	Bolivina plicata	6,8	OS-123677	0,4259	0,0015	6.860	30
96-97	Bolivina plicata	6,8	OS-123678	0,3903	0,0013	7.560	25

Table 3. Reservoir age (DR) estimation considering the ^{210}Pb age determined with the CRS model (McCaffrey and Thomson, 1980) at a selected depth sections of the core, compared with ^{14}C ages (yr BP) from marine13.14 curve (Reimer et al., 2013), according to Sabatier et al. (2010).

Core	cm	Age from CRS model	Age years BP[a]	^{14}C marine13 curve	^{14}C age BP from foram.	DR	s
BGGC5	10.5	1828	122	499	940	441	15
BTCG8	5.5	1908	42	448	890	442	17

a. Before present=1950

Table 4. Spearman rank order correlations for geochemical data. Significant values >0.8 are indicated in bold.

BGGC5

	Al	**P**	**K**	**Ca**	Mn	**Fe**	**Ni**	**Cu**	**Mo**	**Cd**	**Re**	**Sr**	**U**	**Ba**	**Opal**	**TOC**
Al	1.00	-0.62	0.49	-0.48	0.64	0.60	-0.75	0.56	-0.10	-0.73	-0.08	-0.33	0.08	0.49	-0.52	-0.44
P		1.00	-0.31	0.37	-0.45	-0.56	0.56	-0.57	0.01	0.61	-0.11	0.39	-0.12	-0.20	0.49	0.24
K			1.00	-0.24	**0.90**	**0.83**	-0.29	0.47	0.28	-0.42	0.33	-0.12	0.50	0.26	-0.25	-0.19
Ca				1.00	-0.47	-0.50	0.44	-0.64	0.23	0.59	0.39	**0.92**	0.30	-0.60	0.18	0.32
Mn					1.00	**0.94**	-0.51	0.68	-0.01	-0.68	0.07	-0.32	0.24	0.43	-0.39	-0.31
Fe						1.00	-0.49	**0.81**	0.03	-0.70	0.11	-0.40	0.23	0.36	-0.37	-0.21
Ni							1.00	-0.51	0.49	**0.91**	0.35	0.25	0.26	-0.70	0.72	0.64
Cu								1.00	-0.12	-0.71	-0.06	-0.61	0.00	0.31	-0.39	-0.07
Mo									1.00	0.50	**0.88**	0.10	0.91	-0.48	0.33	0.36
Cd										1.00	0.36	0.42	0.27	-0.67	0.70	0.54
Re											1.00	0.27	**0.92**	-0.50	0.16	0.38
Sr												1.00	0.24	-0.36	0.05	0.17
U													1.00	-0.39	0.10	0.29
Ba														1.00	-0.30	-0.59
Opal															1.00	0.35
TOC																1.00

BTGC8

	Al	**P**	**K**	**Ca**	**Mn**	**Fe**	**Ni**	**Cu**	**Mo**	**Cd**	**Re**	**Sr**	**U**	**Ba**	**Opal**	**TOC**
Al	1.00	-0.19	-0.17	-0.37	-0.02	-0.03	-0.39	-0.04	-0.39	0.02	-0.13	-0.58	-0.19	0.07	-0.41	-0.29
P		1.00	0.23	0.00	0.43	0.28	0.58	0.23	0.37	0.13	-0.04	0.30	0.14	-0.14	0.56	0.13
K			1.00	-0.02	0.54	0.41	0.43	0.22	-0.11	0.05	-0.04	0.19	-0.28	0.28	0.26	0.20
Ca				1.00	-0.33	-0.27	0.00	-0.23	0.39	0.01	0.33	0.50	0.47	-0.34	0.20	0.34
Mn					1.00	0.21	0.64	0.01	0.05	0.33	0.15	0.32	-0.02	0.24	0.32	0.00
Fe						1.00	0.13	0.71	-0.40	-0.48	-0.67	-0.37	-0.62	0.13	0.14	0.10
Ni							1.00	0.24	0.56	0.20	0.25	0.64	0.19	-0.16	**0.80**	0.45
Cu								1.00	-0.25	-0.68	-0.56	-0.22	-0.61	-0.10	0.21	0.37
Mo									1.00	0.45	0.59	0.66	0.69	-0.41	0.58	0.30
Cd										1.00	0.56	0.39	0.52	0.11	0.10	-0.12
Re											1.00	0.53	**0.83**	-0.16	0.13	0.17
Sr												1.00	0.58	-0.13	0.52	0.23
U													1.00	-0.19	0.21	0.00
Ba														1.00	-0.28	-0.42
Opal															1.00	0.39
TOC																1.00

Figures

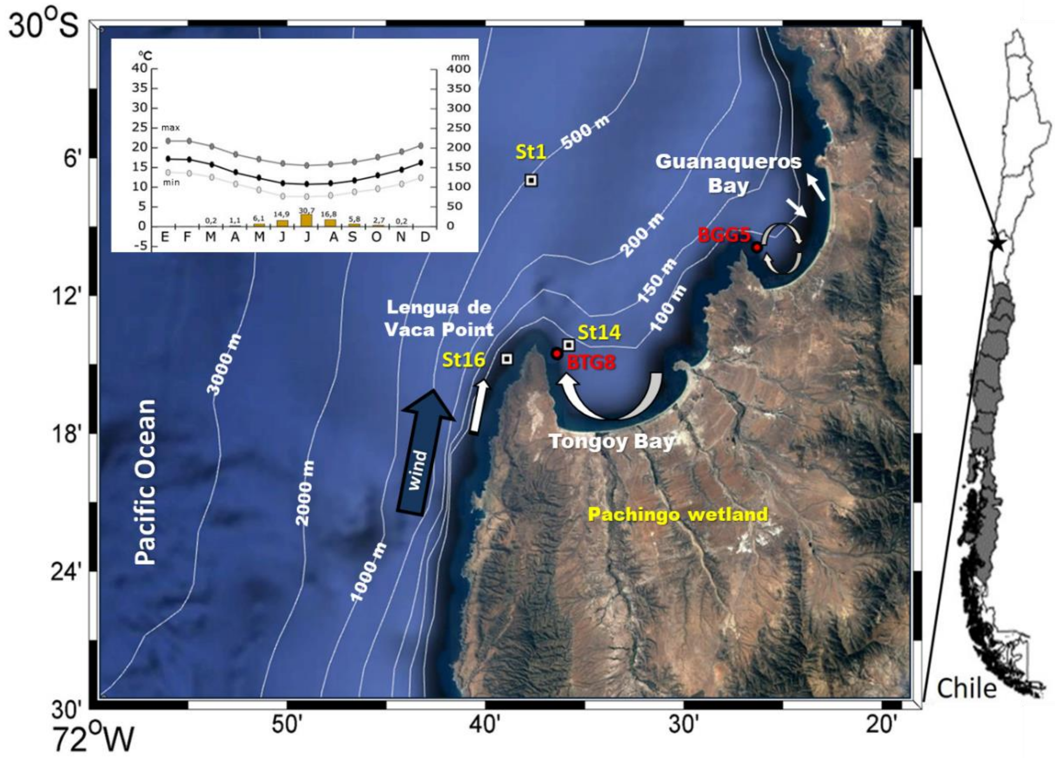

Figure 1. Study area showing the position of sampling stations. Sediment cores were retrieved from Guanaqueros Bay (BGGC5) and from Tongoy Bay (BTGC8) at water depths of 89 and 85 m, respectively. Information of dissolved oxygen (DO) in the water column at ST1and ST16 and of suspended organic particles collected at ST14 sampling sites was gathered in a previous project (INNOVA 07CN13 IXM-150). Climograph of the region is showing the average precipitation in mm (bars) and temperatures in °C (min, max and average) over 12-month period. Schematic representation of the bays circulation (white arrows) and wind direction is indicated (blue arrow) obtained from Valle-Levinson and Moraga-Opazo (2006) and Moraga-Opazo et al. (2001).

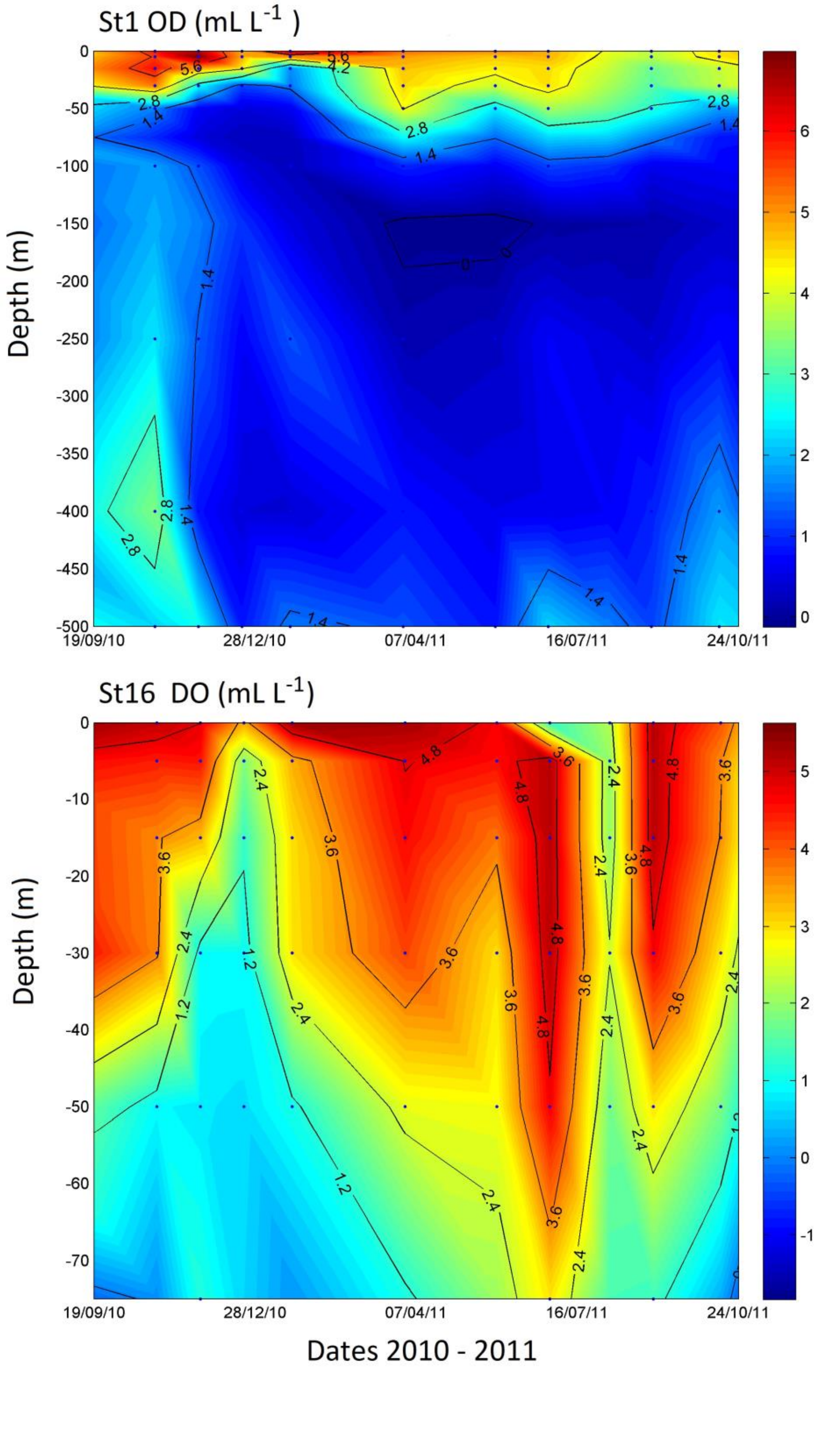

Figure 2. Dissolved Oxygen (DO) time series in the water column measured between October 2010 and January 2011, at stations St1 and St16 off Tongoy Bay, Coquimbo (30°S).

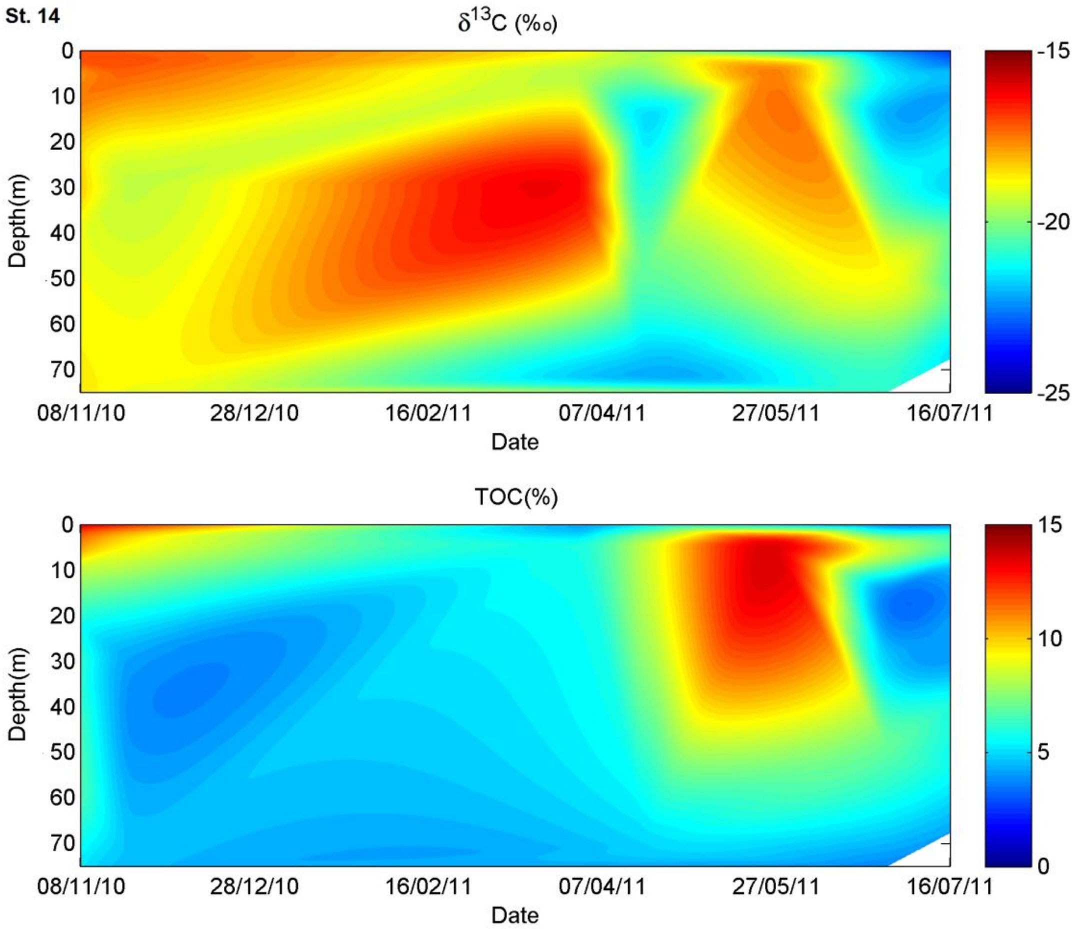

Figure 3. Suspended particulate matter composition (TOC % and δ^{13}Corg) measured in the water column between October 2010 and October 2011, at station St14, Tongoy Bay, Coquimbo (30°S).

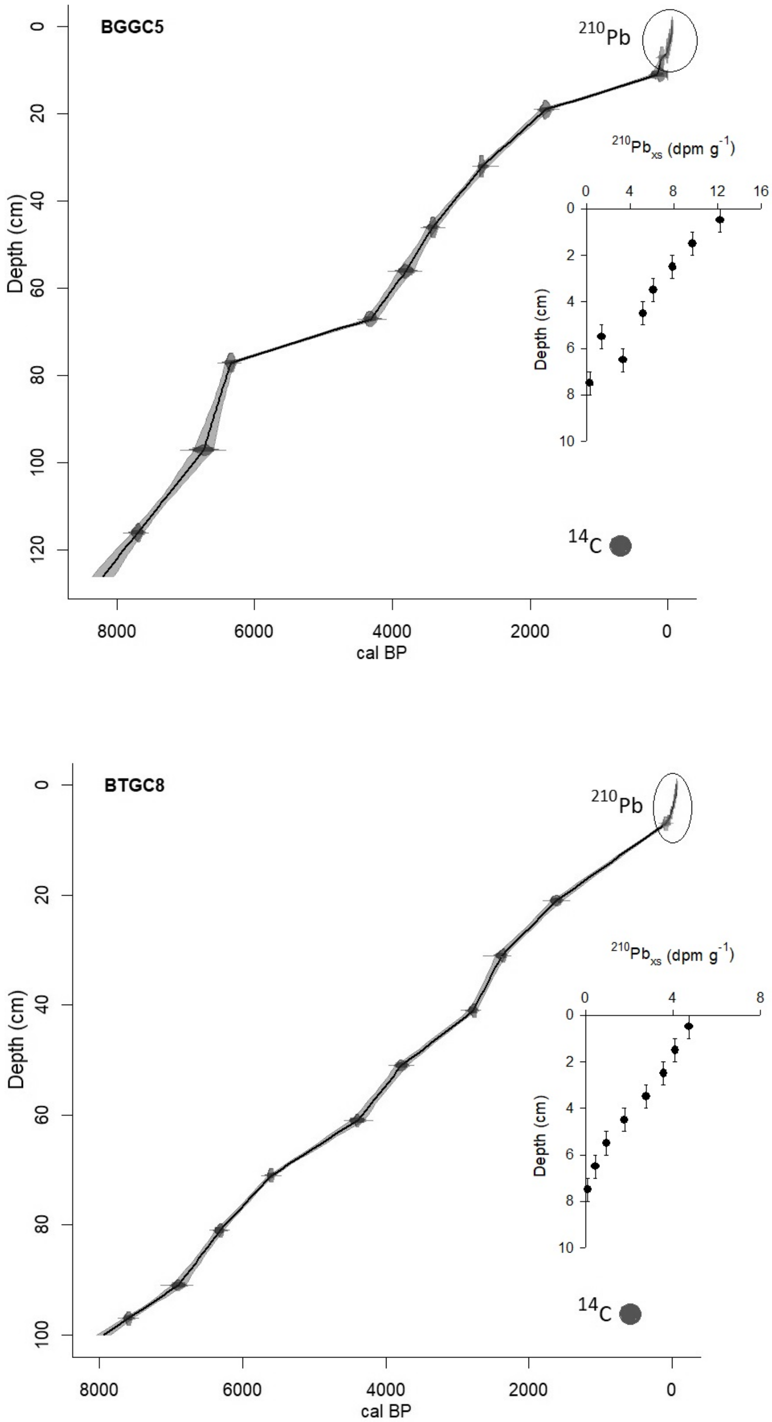

Figure 4. Age model based on ^{14}CAMS and ^{210}Pb measurements. The time scale was obtained according to the best fit of curves of $^{210}Pb_{xs}$ and ^{14}C points using CLAM 2.2 software and Marine curve ^{13}C (Reimer et al., 2013).

a) BGGC5

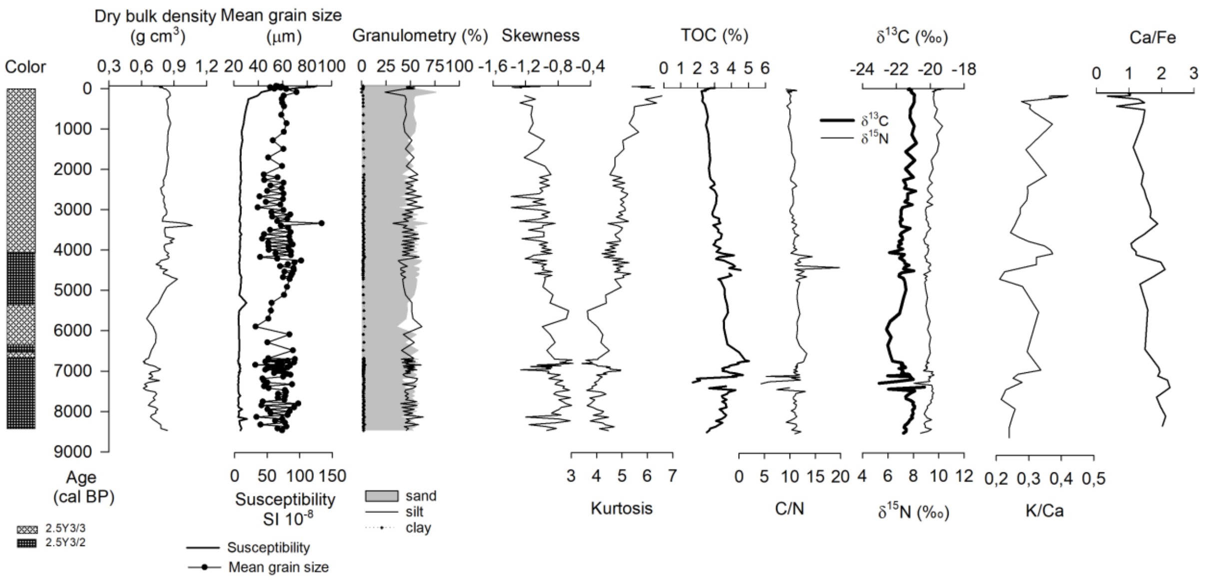

b) BTGC8

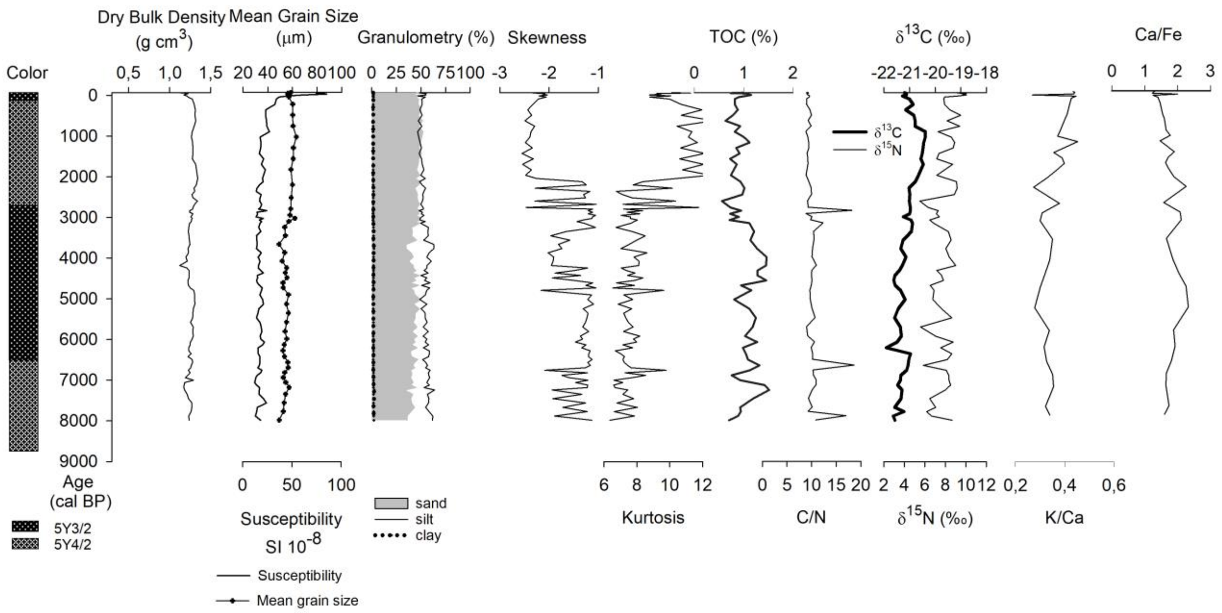

Figure 5. Sediment characterization of sediment cores retrieved from (a) Guanaqueros Bay (BGGC5) and (b) Tongoy Bay (BTGC8). Distribution in depth core of color, dry bulk density, statistical parameters (skewness, mean grain size, kurtosis), organic components (TOC, stable isotopes) and chemical composition (K/Ca, Ca/Fe).

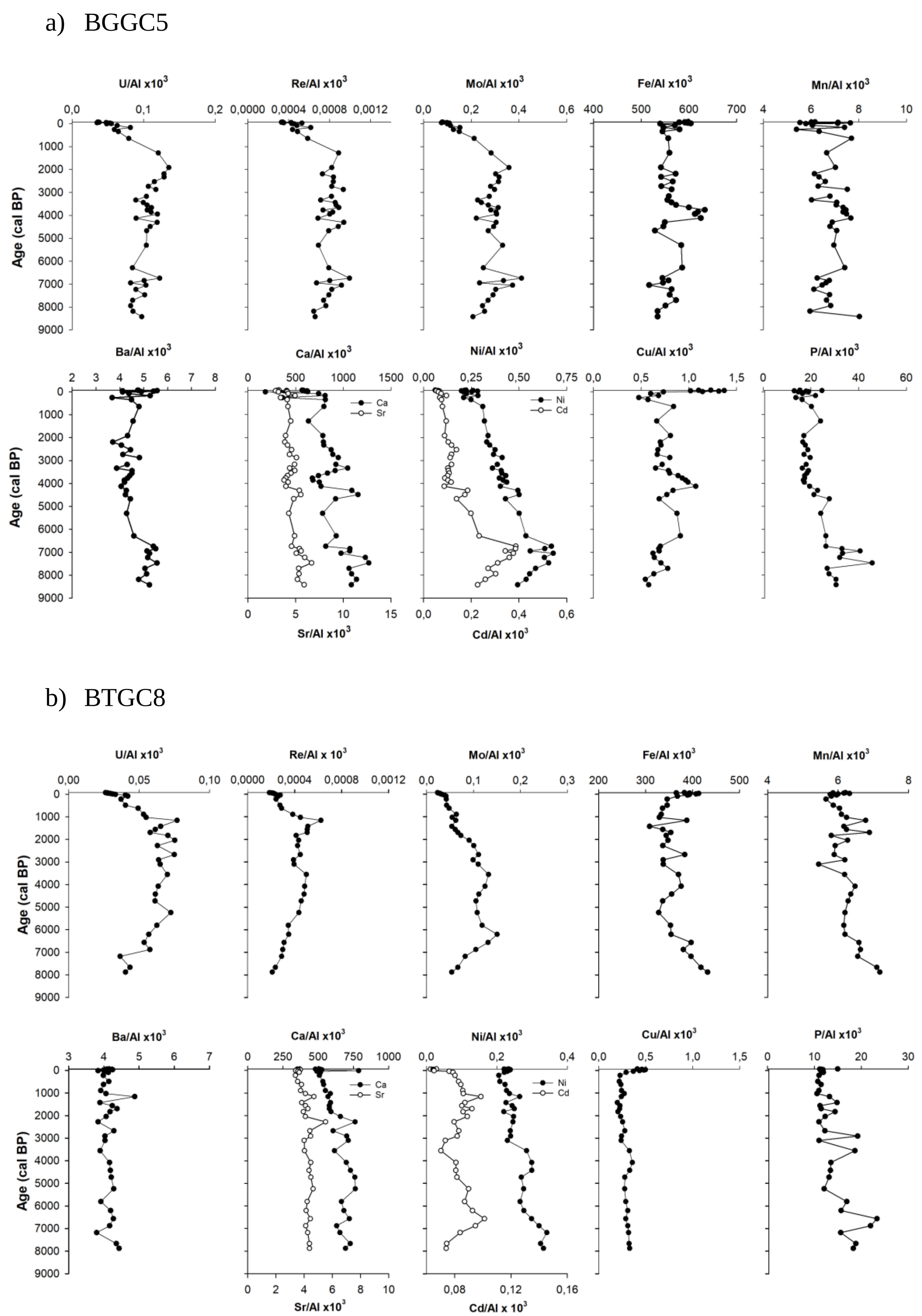

Figure 6. Trace element distribution in sediment cores retrieved from (a) Guanaqueros Bay (BGGC5) and (b) Tongoy Bay (BTGC8), off Coquimbo (30°S).

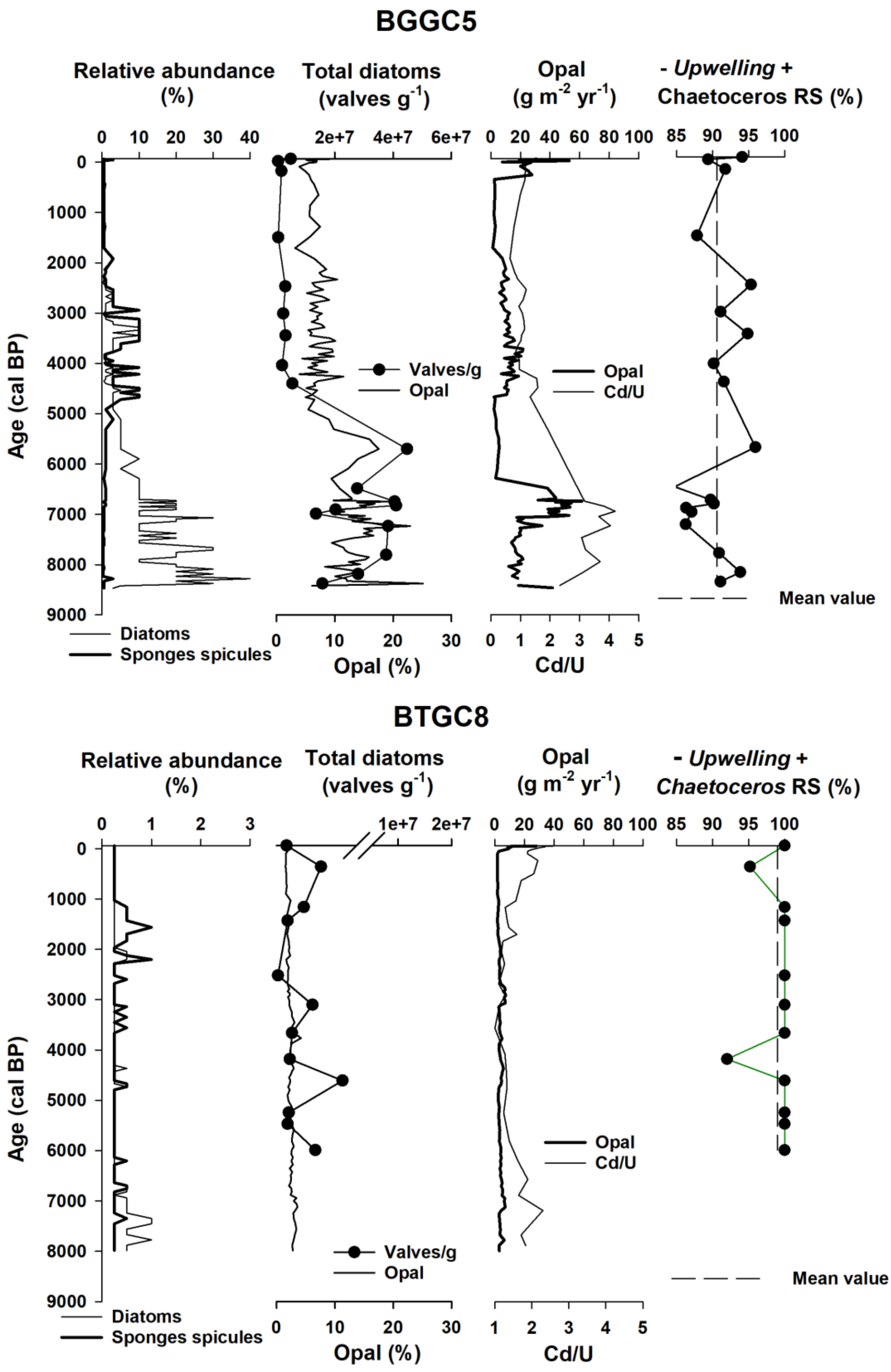

Figure 7. Diatom abundance, opal accumulation and temporal variations in the relative abundance of *Chaetoceros* resting spores in BGGC5 and BTGC8 cores (Guanaqueros and Tongoy Bay, respectively). Cd/U distribution was included as a proxy for redox condition.

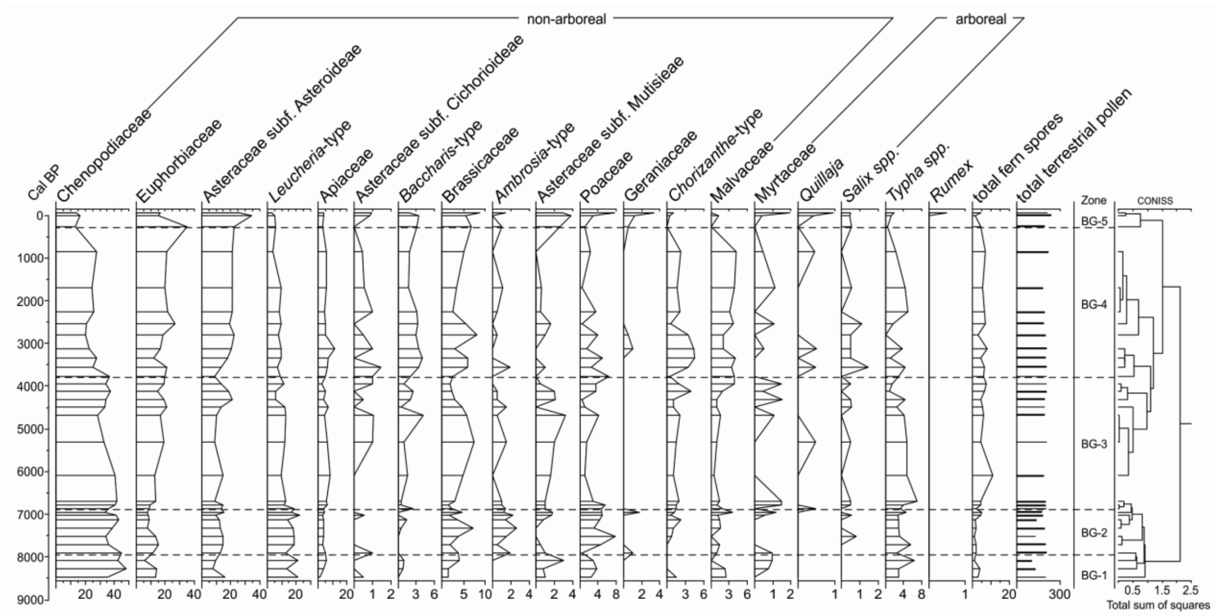

Figure 8. Pollen record in BGGC5 core.

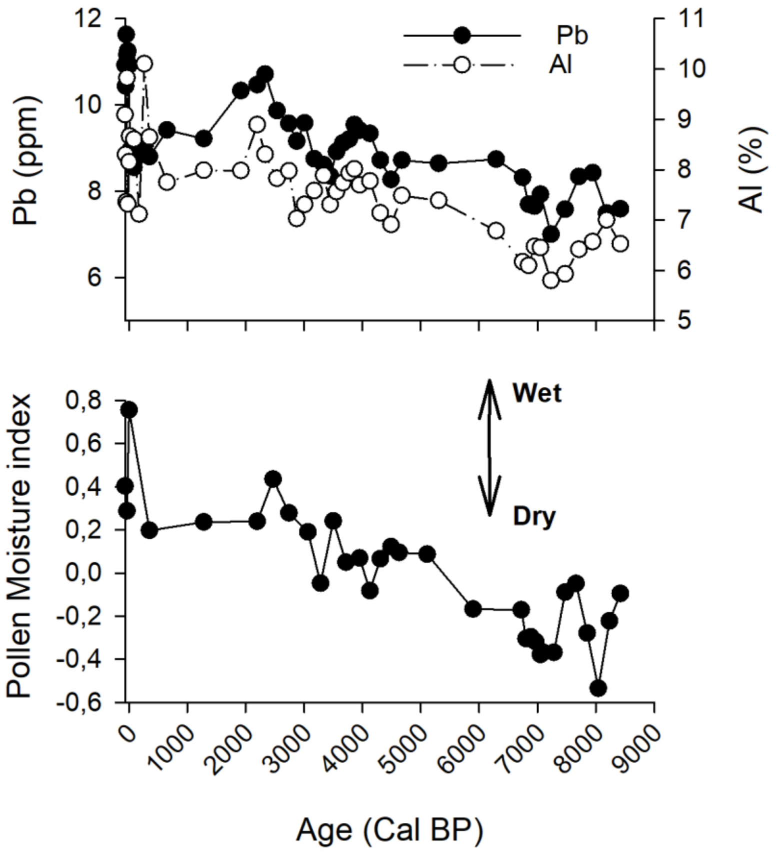

Figure 9. Pollen Moisture Index defined as the normalized ratio between Euphorbiaceae (wet coastal shrub land) and Chenopodiaceae (arid scrubland). Positive (negative) values for this index indicate the relative expansion (reduction) of coastal vegetation under wetter (drier) conditions. Pb and Al distribution at BGGC5 core, representatives of terrigenous input to the bay.